Structural Engineering and Mechanics, *Vol. 76, No. 1 (2020) 27-56*
DOI: https://doi.org/10.12989/sem.2020.76.1.027

Size dependent effect on deflection and buckling analyses of porous nanocomposite plate based on nonlocal strain gradient theory

Pegah Khazaei[1] and Mehdi Mohammadimehr*

Department of Solid Mechanics, Faculty of Mechanical Engineering, University of Kashan, P.O. Box: 87317-53153, Kashan, Iran

(Received August 19, 2019, Revised November 15, 2019, Accepted May 18, 2020)

Abstract. In this paper, the deflection and buckling analyses of porous nano-composite piezoelectric plate reinforced by carbon nanotube (CNT) are studied. The equations of equilibrium using energy method are derived from principle of minimum total potential energy. In the research, the non-local strain gradient theory is employed to consider size dependent effect for porous nanocomposite piezoelectric plate. The effects of material length scale parameter, Eringen's nonlocal parameter, porosity coefficient and aspect ratio on the deflection and critical buckling load are investigated. The results indicate that the effect of porosity coefficient on the increase of the deflection and critical buckling load is greatly higher than the other parameters effect, and size effect including nonlocal parameter and the material length scale parameter have a lower effect on the deflection increase with respect to the porosity coefficient, respectively and vice versa for critical buckling load. Porous nanocomposites are used in various engineering fields such as aerospace, medical industries and water refinery.

Keywords: deflection and buckling analyses; porous materials; nanocomposite; carbon nanotube; nonlocal strain gradient theory; principle of minimum total potential energy

1. Introduction

Nanoscience refers to the study of various structures such as beam, plate, and shell at the scale of nanometers that has different applications such as chemistry, physics, biology and engineering. Nanocomposite plates are one of the most important topic in the nanoscience studies. Carbon nanotubes (CNTs) are kind of reinforcement that are used in polymer composites as their special mechanical properties including low density, high stiffness and tensile strength. Porous materials are the one type of lightweight materials. In porous plates, porosity can vary along the thickness and leads to change the mechanical properties of structures. For instance, porous nanocomposite filters can be used to disinfect water.

Using Hamilton's principle, Jomehzadeh *et al.* (2011) proposed vibration analysis of micro-plates based on size-dependent effect including modified couple stress theory (MCST). Based on classical plate theory (CPT), Yin *et al.* (2010) and Wang *et al.* (2011) presented vibration analysis of microscale plates based on modified couple stress theory (MCST) and a size-dependent Kirchhoff micro-plate model based on strain gradient elasticity theory (SGT), respectively. Thai and Choi (2013) investigated size-dependent effect on bending, buckling and vibration analyses of functionally graded (FG) CPT and Mindlin plates using MCST. Using energy method, Mohammadimehr *et al.* (2016a) illustrated surface stress effect on the bending and vibration analyses of single-layer graphene sheet on elastic foundation based on nonlocal elasticity theory. Also, using Hamilton's principle and modified general strain gradient theory (MGSGT), Mohammadimehr *et al.* (2018) studied the buckling and vibrations analysis of double-bonded micro composite sandwich plates reinforced by CNTs and boron nitride nanotubes (BNNTs) with isotropic foam and flexible transversely orthotropic cores. Ghorbanpour Arani *et al*. (2016) presented surface stress and agglomeration effects on nonlocal biaxial buckling polymeric nanocomposite plate reinforced by CNT using various approaches.

Also, a nonlocal strain gradient theory has been done by the following researchers:

Lu *et al.* (2017) depicted vibration analysis of nanobeams based on the nonlocal strain gradient theory (NSGT). Ebrahimi *et al.* (2018) used the damping vibration analysis of graphene sheets on viscoelastic medium with considering hygro-thermal effects employing NSGT. Malikan *et al.* (2018) studied damped forced vibration analysis of single-walled carbon nanotubes (SWCNTs) resting on visco-elastic foundation using NSGT in thermal environment. She *et al.* (2018) investigated nonlinear bending and vibration analyses of FG porous tubes via NSGT. Apuzzo *et al.* (2018) illustrated free vibrations of beams by modified NSGT. Lu *et al.* (2019) presented a unified size-dependent plate model based on NSGT including surface effects. Arefi *et al.* (2019) considered bending analysis of a sandwich porous nanoplate integrated with piezomagnetic face-sheets using NSGT. Mahinzare *et al.* (2019) proposed a NSGT for dynamic modeling of a rotary thermo-piezo electrically actuated nano FG circular plate.

In order to consider a different approach on studying nanoplates, Barretta *et al*. (2019) illustrated that the stress-

*Corresponding author, Ph.D.
E-mail: mmohammadimehr@kashanu.ac.ir

ISSN: 1225-4568 (Print), 1598-6217 (Online)

driven approach can be employed as an alternative for the design of modern nano-structured components of Nano-Electro-Mechanical Systems (NEMS). Mohammadimehr *et al*. (2017b) illustrated dynamic stability of modified strain gradient theory sinusoidal viscoelastic piezoelectric polymeric functionally graded single-walled carbon nanotubes reinforced nanocomposite plate considering surface stress and agglomeration effects under hydro-thermo-electro-magneto-mechanical loadings. In the other work, they (2016d) considered size-dependent effect on biaxial and shear nonlinear buckling analysis of nonlocal isotropic and orthotropic micro-plate based on surface stress and modified couple stress theories using differential quadrature method.

In the field of porosity, Rezaei and Saidi (2015) indicated free vibration analysis for thick porous plate saturated by inviscid fluid based on Reddy plate theory. Also, Kim *et al.* (2019) investigated bending, free vibration, and buckling of FG porous micro-plates using MCST. Further, Yang *et al.* (2018) inquired buckling and free vibration analyses of FG graphene reinforced porous nano-composite plates based on Chebyshev-Ritz method. Among the studies in the field of piezoelectric nanocomposites, these probes can be noted (Arani *et al.* (2016), Gholami and Ansari (2017), Tanzadeh and Amoushahi (2019) and Mao and Zhang (2019), Rajabi and Mohammadimehr (2019)). Moreover, for checking out the different distribution patterns of CNTs, using modified strain gradient theory (MSGT), Mohammadimehr *et al.* (2016b) proposed Reddy rectangular plate model for biaxial buckling and bending analyses of double-bonded piezoelectric polymeric nanocomposite reinforced by FG-SWCNT. Also, Sofiyev *et al.* (2019) presented an analytical solution for the stability problem of FG-CNT reinforced composite (FG-CNTRC) conical shells (CSs). The materials of FGCNTRC-CSs are graded in the thickness direction according to linear distributions of the volume fraction of CNTs. The results indicated that the minimum and maximum FG effect belonged to the FG-V and FG-X distribution patterns, respectively. To study material length scale parameter, Thai and Kim (2013) illustrated that small scale effects are important when the plate thickness is small, though when plate thickness increases small scale effects become negligible. Also, Alizada and Sofiyev (2011) obtained the modified Young's moduli for the two-dimensional single crystal body with a square lattice. Their results showed that the influences of scale effects and vacancies on the Young's moduli are considerable. In addition, they showed that the effective Young's moduli have three components including the macroscopic value; factors determining the scale effect; factors determining the vacancy. The last component is analogous to the parameter of the damage of fracture theory.

Many researchers have studied dynamic response, deflection and buckling of plates considering different plate theories as follows:

Based on higher order shear and normal deformable plate theories, plane wave solutions and modal analysis, vibrations of thick isotropic plates, FG incompressible linear elastic plates, and vibration of an incompressible isotropic plate have been considered by Batra *et al.* (2002), Batra and Aimmanee (2005), Batra (2007), Batra and Aimmanee (2007), respectively. Aghababaei and Reddy (2009) investigated nonlocal elasticity theory as well as third-order shear deformation theory (TSDT) with application to bending and vibration of plates. Saidi *et al*. (2009) taken into account bending and buckling analyses of thick FG circular plates using unconstrained TSDT. Based on shear deformation theory, Reddy (2010) presented bending of beams and plates based on nonlocal nonlinear formulations. Also, Reddy and Kim (2012) considered a nonlinear kinematic equations of FG plates based on MCST and TSDT. In another work, they illustrated analytical solutions for bending, vibration, and buckling of FGM plates using MCST and TSDT. Mohammadimehr *et al*. (2017a) presented nonlinear vibration analysis of FG-CNTRC sandwich Timoshenko beam based on modified couple stress theory subjected to longitudinal magnetic field using generalized differential quadrature method. Using nonlocal Mindlin-plate, Arani *et al.* (2012) illustrated buckling analysis and smart control of SLGS using elastically coupled PVDF nanoplate. Rezaei *et al.* (2017) studied the natural frequencies of FG plates with porosities using four variable plate theories. Using sinusoidal shear deformation theory (SSDT), MSGT, and meshless method, Mohammadimehr *et al.* (2015) presented free vibration of viscoelastic double-bonded polymeric nano-composite plates reinforced by FG-SWCNTs. Mohammadimehr *et al.* (2016c) investigated bending, buckling, and vibration analyses of micro-composite plate reinforced by FG-SWCNTs with material properties of temperature-dependent under combined loadings using DQM. Van *et al.* (2017) presented bi-directional FG plates by FEM and a new TSDT. Using SSDT, Arani and Jalaei (2017) investigated dynamic response of viscoelastic graphene sheet based on the effect of longitudinal magnetic field. Using hyperbolic shear deformation theory, Zenkour and Radwan (2018) considered FG plates on elastic foundations under various boundary conditions. Akhavan Alavi *et al*. (2019) considered active control of micro Reddy beam integrated with FG nanocomposite sensor and actuator based on linear quadratic regulator method. Zenkour and Alghanmi (2019) showed stress analysis of a FG plate integrated with piezoelectric faces. Ebrahimi *et al.* (2019) presented the characteristics of wave dispersion for porous composite shell reinforced by graphene platelet. Mohammadimehr and Alimirzaei (2016) presented nonlinear static and vibration analysis of Euler-Bernoulli composite beam model reinforced by FG-SWCNT with initial geometrical imperfection using FEM.

Mohammadzadeh *et al.* (2019) illustrated vibration of sandwich plates on elastic foundation and considering the temperature change and FGM face-sheet layers. Alavi and Eipakchi (2019) studied transient response of a VFGM annular plate based on_geometry and load effects. Using Cooper-Naghdi theory, Yazdani *et al.* (2019) presented vibration of micro saturated porous sandwich cylindrical shells reinforced by CNT as face sheets layers under combined loadings.

According to the aforesaid researches, deflection and buckling analysis of the nanocomposite plate have been

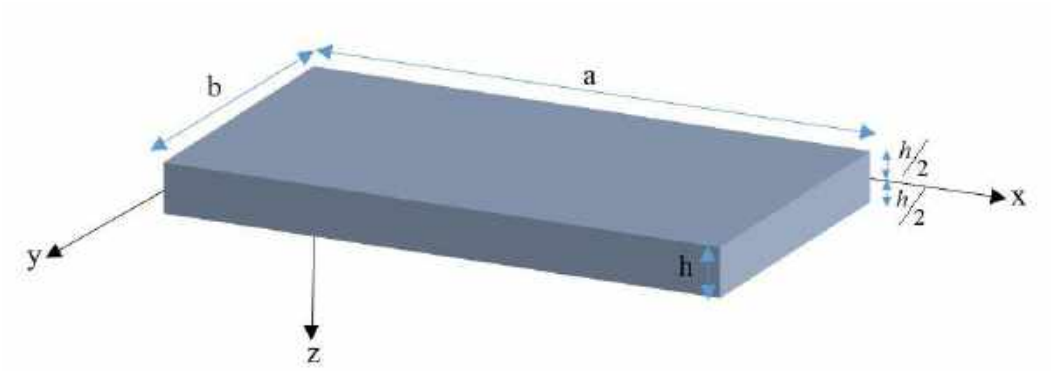

Fig. 1 A schematic view of porous nanocomposite piezoelectric plate reinforced by FG-SWCNTs

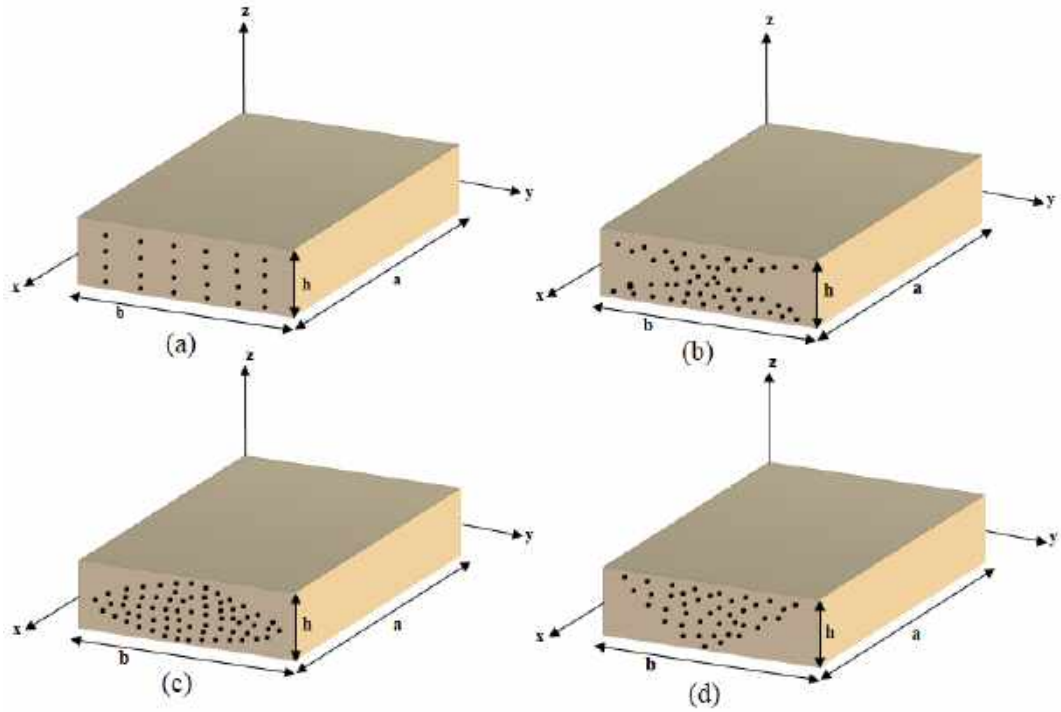

Fig. 2 A schematic view of various distributions of CNTs

developed and investigated many times, but no literature has been reported for deflection and buckling analysis of porous nanocomposite piezoelectric plate based on nonlocal strain gradient theory. In this article, the effects of size dependent including material length scale parameter, Eringen's nonlocal parameter, porosity and aspect ratio on the deflection and critical buckling load are taken into account.

2. Geometry and simulation

Consider a porous nanocomposite piezoelectric plate reinforced by FG-SWCNTs which its length, width and thickness are *a*, *b* and *h*, respectively as showed in Figs. 1, 2.

The different distribution patterns of SWCNTs along thickness direction have been illustrated in Fig. 2. According to this figure, these patterns are a) uniform distribution (UD), b) FG-X, c) FG-O d) FG-V. Various volume fraction distributions of SWCNTs can be represented as follows (Shen and Zhang (2010), Zhu *et al.* (2012)):

$$V_{CNT}(z)=\begin{cases} V_{CNT}^{*} & (UD \quad CNTRC) \\ \left(1+\dfrac{2z}{h}\right)V_{CNT}^{*} & (FG-V \quad CNTRC) \\ 2\left(1+\dfrac{|2z|}{h}\right)V_{CNT}^{*} & (FG-O \quad CNTRC) \\ V_{r}=2\dfrac{|2z|}{h}V_{CNT}^{*} & (FG-X \quad CNTRC) \end{cases} \tag{1}$$

where

$$V_{CNT}^{*}=\frac{w_{CNT}}{w_{CNT}+\left(\rho^{CNT}/\rho^{m}\right)-\left(\rho^{CNT}/\rho^{m}\right)w_{CNT}} \tag{2}$$

In which ρ^{CNT} and ρ^{m} are the densities of SWCNTs and Polyvinylidene fluoride (PVDF) nanoplate matrix, respectively and w_{CNT} is the mass fraction of nanotube.

3. Material properties

3.1 The extended rule of mixture approach

In this study, the extended rule of mixture (ERM) approach has been employed to consider nano-composite properties reinforced by CNTs. Based on this model, the mechanical properties of SWCNTs-reinforced composite nanoplate are obtained from the following equations (Shen (2009) and Shen and Zhang (2010)):

$$E_{11} = \eta_1 V_{CNT} E_{11}^{CNT} + V_m E_m$$

$$\frac{\eta_2}{E_{22}} = \frac{V_{CNT}}{E_{22}^{CNT}} + \frac{V_m}{E_m} \tag{3}$$

$$\frac{\eta_3}{G_{12}} = \frac{V_{CNT}}{G_{12}^{CNT}} + \frac{V_m}{G_m}$$

where E_{11}^{CNT}, E_{22}^{CNT} and G_{12}^{CNT} introduce Young's modulus (in various directions) and shear modulus of SWCNTs, respectively, and E_m and G_m are the elasticity modulus related to PVDF matrix. $\eta_i (i = 1,2,3)$ is CNT efficiency parameter which specified by molecular dynamic (MD) simulation. In fact, CNT efficiency parameters are the transformation forces between carbon nanotubes and matrix. V_m is volume fractions of PVDF nanoplate matrix. The relation between volume fractions of CNT and PVDF nanoplate matrix is defined by (Shen (2009)):

$$V_{CNT} + V_m = 1 \tag{4}$$

Also, the Poisson's ratio along the thickness direction and density of the composite plate are given by the following equations (Shen (2009)):

$$\upsilon = V_{CNT}^{*} \upsilon^{CNT} + V_m \upsilon^{m} \tag{5}$$

$$\rho = V_{CNT} \rho^{CNT} + V_m \rho^{m} \tag{6}$$

where υ^{m} and υ^{CNT} are Poisson's ratio of PVDF nanoplate matrix and SWCNTs, respectively.

The values of properties of SWCNTs and PVDF nanoplate matrix and CNT efficiency parameters are depicted in Tables 1-3.

3.2 Porous composite nanoplate

Due to the porosity of the composite nanoplate, density and elasticity modulus of the mentioned plate are functions of the z because distribution of porosity along the thickness of plate is variable. Thus, the density and elasticity modulus of FG-SWCNTs-reinforced porous composite nanoplate are obtained by following equations (Magnucka-Blandzi (2008)):

Table 1 Properties of SWCNTs and PVDF nanoplate matrix (Shen 2009)

SWCNTs	PVDF
-	$E_m = (3.51 - 0.0047T)(GPa)$ $T = T_0 + \Delta T(K)$ $G_m = \frac{E_m}{2(1+\nu_m)}(GPa)$
$\upsilon_{CNT} = 0.175$	$\upsilon_m = 0.18$
$V_{CNT} = 0.11$	$V_m = 0.89$
$\rho_{CNT} = 1400\left(\frac{kg}{m^3}\right)$	$\rho_m = 1780\left(\frac{kg}{m^3}\right)$

Table 2 Mechanical properties of SWCNTs with $\upsilon_{CNT} = 0.175$ (Shen 2009)

Temperature $(T_0)(K)$	$E_{11}^{CNT}(TPa)$	$E_{22}^{CNT}(TPa)$	$G_{12}^{CNT}(TPa)$
300	5.6466	7.0800	1.9445
400	5.5308	6.9348	1.9643
500	5.4744	6.8641	1.9644

Table 3 CNT efficiency parameters (Shen 2009)

V_{CNT}^{*}	η_1	η_2	η_3
0.11	0.149	0.934	0.934
0.14	0.150	0.941	0.941
0.17	0.149	1.381	1.381

$$\begin{cases} E_x(z) = E_{11}\left(1\text{-}e_0\cos\left(\frac{\pi}{2h}(z+\frac{h}{2})\right)\right) \\ E_y(z) = E_{22}\left(1\text{-}e_0\cos\left(\frac{\pi}{2h}(z+\frac{h}{2})\right)\right) \\ E_{xy}(z) = G_{12}\left(1\text{-}e_0\cos\left(\frac{\pi}{2h}(z+\frac{h}{2})\right)\right) \\ \rho(z) = \rho\left(1\text{-}e_0'\cos\left(\frac{\pi}{2h}(z+\frac{h}{2})\right)\right) \\ e_0' = 1-\sqrt{1-e_0} \end{cases} \tag{7}$$

In which, e_0 is porosity coefficient and the values of E_{11}, E_{22}, G_{12} and ρ are embedded using relations (3) and (6).

4. Formulation

Using energy method and minimum total potential energy principle, the governing equations of equilibrium are derived by considering displacement fields, strain-displacement equations of classical plate theory (CPT) and stress-strain equations of FG-CNT-reinforced piezoelectric and porous nanocomposite plate.

The displacement fields for classical plate theory with Cartesian coordinates in *x, y* and *z* directions which can be represented by $u_1(x,y,z)$, $u_2(x,y,z)$ and $u_3(x,y,z)$ respectively, can be written as follows (Reddy 2017):

$$\begin{cases} u_1(x,y,z)=u_0(x,y)-z\dfrac{\partial w(x,y)}{\partial x} \\ u_2(x,y,z)=v_0(x,y)-z\dfrac{\partial w(x,y)}{\partial y} \\ u_3(x,y,z)=w(x,y) \end{cases} \tag{8}$$

According to equation (8), the strain-displacement relations of the CPT are as follows (Reddy 2017):

$$\begin{cases} \varepsilon_{xx}=\dfrac{\partial u_1}{\partial x}=\dfrac{\partial u_0}{\partial x}-z\dfrac{\partial^2 w}{\partial x^2} \\ \varepsilon_{yy}=\dfrac{\partial u_2}{\partial y}=\dfrac{\partial v_0}{\partial y}-z\dfrac{\partial^2 w}{\partial y^2} \\ \gamma_{xy}=\dfrac{\partial u_1}{\partial y}+\dfrac{\partial u_2}{\partial x}=\dfrac{\partial u_0}{\partial y}+\dfrac{\partial v_0}{\partial x}-2z\dfrac{\partial^2 w}{\partial x\,\partial y} \end{cases} \tag{9}$$

4.1 Nonlocal strain gradient theory for porous nanocomposite piezoelectric plate

The constitutive equations of FG-SWCNTs-reinforced porous nanocomposite piezoelectric plate are as follows (Li *et al.* 2016):

$$\begin{cases} \left(1-(ea)^2\nabla^2\right)\sigma_{xx}=\left(1-\ell^2\nabla^2\right)\left(q_{11}\varepsilon_{xx}+q_{12}\varepsilon_{yy}\right)-e_{31}E_z \\ \left(1-(ea)^2\nabla^2\right)\sigma_{yy}=\left(1-\ell^2\nabla^2\right)\left(q_{12}\varepsilon_{xx}+q_{22}\varepsilon_{yy}\right)-e_{32}E_z \\ \left(1-(ea)^2\nabla^2\right)\tau_{xy}=\left(1-\ell^2\nabla^2\right)q_{66}\gamma_{xy} \end{cases} \tag{10-a}$$

where ℓ and ea are material length scale and Eringen's nonlocal parameters, respectively.

Based on equations in Appendix C, the classical boundary conditions including essential and natural boundary conditions with simply supported edges are obtained as follows:

$$\begin{aligned} &x=0,a \\ &u_0=0 \text{ or } N_x=0 \\ &v_0=0 \text{ or } N_{xy}=0 \end{aligned} \tag{10-b}$$

$$\begin{aligned} &y=0,b \\ &v_0=0 \text{ or } N_y=0 \\ &u_0=0 \text{ or } N_{xy}=0 \end{aligned} \tag{10-c}$$

$$\begin{aligned} &x=0,a \\ &w_{,x}=0 \text{ or } M_x=0 \\ &w=0 \text{ or } M_{x,x}=0 \\ &w_{,y}=0 \text{ or } M_{xy}=0 \end{aligned} \tag{10-d}$$

$$\begin{aligned} &y=0,b \\ &w_{,y}=0 \text{ or } M_y=0 \\ &w=0 \text{ or } M_{y,y}=0 \\ &w=0 \text{ or } M_{xy,x}=0 \end{aligned} \tag{10-e}$$

The curvatures for rectangular plates are equivalent to the following stress-driven nonlocal differential equation (Barretta Sciarra 2018 and Barretta *et al*. 2019)

$$k_x-L_C{}^2\frac{\partial^2 k_x}{\partial x^2}=\frac{M_x-\upsilon M_y}{D(1-\upsilon^2)},\qquad k_y-L_C{}^2\frac{\partial^2 k_y}{\partial y^2}=\frac{M_y-\upsilon M_x}{D(1-\upsilon^2)} \tag{10-f}$$

where

$$k_x=-w_{,xx}\qquad k_y=-w_{,yy} \tag{10-g}$$

The constitutive boundary conditions for rectangular plate are defined as follows (Barretta Sciarra 2018 and Barretta *et al*. 2019):

$$\begin{aligned} &\frac{\partial k_x}{\partial x}(x=0)=\frac{1}{L_C}k_x(x=0) \\ &-\frac{\partial k_x}{\partial x}(x=a)=\frac{1}{L_C}k_x(x=a) \\ &\frac{\partial k_y}{\partial y}(y=0)=\frac{1}{L_C}k_y(y=0) \\ &-\frac{\partial k_y}{\partial y}(y=b)=\frac{1}{L_C}k_y(y=b) \end{aligned} \tag{10-h}$$

Using above equations, the resultant moments based on stress-driven nonlocal differential equations for rectangular nano plate are obtained as (Barretta *et al*. 2019):

$$\begin{aligned} M_x&=D(k_x+\upsilon k_y-L_C{}^2\frac{\partial^2 k_x}{\partial x^2}-\upsilon L_C{}^2\frac{\partial^2 k_y}{\partial y^2}) \\ M_y&=D(k_y+\upsilon k_x-\upsilon L_C{}^2\frac{\partial^2 k_x}{\partial x^2}-L_C{}^2\frac{\partial^2 k_y}{\partial y^2}) \end{aligned} \tag{10-i}$$

Also for the piezoelectric property of this plate, the electric displacement-electric field relation is considered as follows (Wang 2002):

$$\begin{cases} \left(1-(ea)^2\nabla^2\right)D_x=\xi_{11}E_x \\ \left(1-(ea)^2\nabla^2\right)D_y=\xi_{22}E_y \\ \left(1-(ea)^2\nabla^2\right)D_Z=e_{31}\varepsilon_{xx}+e_{32}\varepsilon_{yy}+\xi_{33}E_z \end{cases} \tag{11}$$

In which D_x, $D_y$and D_Z are electric displacements and E_x, E_y and E_Z are electric fields in *x, y* and *z* directions. Due to Wang (2002) electric-field equations are as follows:

$$\begin{cases} E=-\nabla\Phi \\ \Phi=-\cos(\beta' z)\phi_E(x,y)+\dfrac{2z}{h}V_E \end{cases} \tag{12}$$

$$\begin{cases} E_x=-\dfrac{\partial\Phi}{\partial x}=\cos(\beta' z)\dfrac{\partial\phi_E}{\partial x} \\ E_y=-\dfrac{\partial\Phi}{\partial y}=\cos(\beta' z)\dfrac{\partial\phi_E}{\partial y} \\ E_z=-\dfrac{\partial\Phi}{\partial y}=-\beta'\sin(\beta' z)\phi_E-\dfrac{2V_E}{h} \\ \beta'=\pi/h \end{cases} \tag{13}$$

where V_E is external electric voltage.

Equations (10-a) and (11) can be expressed as follows:

$$\left(1-(ea)^2\nabla^2\right)\begin{Bmatrix}\sigma_{xx}\\ \sigma_{yy}\\ \tau_{xy}\end{Bmatrix}=\left(1-\ell^2\nabla^2\right)\begin{bmatrix}q_{11}&q_{12}&0\\ q_{12}&q_{22}&0\\ 0&0&q_{66}\end{bmatrix}\begin{Bmatrix}\varepsilon_{xx}\\ \varepsilon_{yy}\\ \gamma_{xy}\end{Bmatrix}-\begin{bmatrix}0&0&e_{31}\\ 0&0&e_{32}\\ 0&0&0\end{bmatrix}\begin{Bmatrix}E_x\\ E_y\\ E_z\end{Bmatrix} \tag{14}$$

$$\left(1-(ea)^2\nabla^2\right)\begin{Bmatrix}D_x\\D_y\\D_z\end{Bmatrix}=\begin{bmatrix}0&0&0\\0&0&0\\e_{31}&e_{32}&0\end{bmatrix}\begin{Bmatrix}\varepsilon_{xx}\\\varepsilon_{yy}\\\gamma_{xy}\end{Bmatrix}+\begin{bmatrix}\xi_{11}&0&0\\0&\xi_{22}&0\\0&0&\xi_{33}\end{bmatrix}\begin{Bmatrix}E_x\\E_y\\E_z\end{Bmatrix} \quad (15)$$

where

$$\begin{cases}q_{11}(z)=\dfrac{E_x(z)}{1-\upsilon_{12}\upsilon_{21}} & q_{12}(z)=\dfrac{\upsilon_{21}E_x(z)}{1-\upsilon_{12}\upsilon_{21}}\\ q_{22}(z)=\dfrac{E_y(z)}{1-\upsilon_{12}\upsilon_{21}} & q_{66}(z)=E_{xy}(z)\end{cases} \quad (16)$$

In which e_{31} , e_{32} , ξ_{11} , ξ_{22} and ξ_{33} are listed in Table 4 (Arani *et al.* (2016)):

Table 4 Piezoelectric properties of PVDF (Arani *et al*. 2016)

$e_{31}\left(\frac{C}{m^2}\right)$	$e_{32}\left(\frac{C}{m^2}\right)$	$\xi_{11}\left(\frac{F}{m}\right)$	$\xi_{22}\left(\frac{F}{m}\right)$	$\xi_{33}\left(\frac{F}{m}\right)$
-0.13	-0.145	1.1068e-8	1.1067e-8	1.1067e-8

4.2 Governing equations of equilibrium

In this study, energy method is used to obtain governing equations of equilibrium. In the energy method, the total potential energy (Π) is obtained from the strain energy (U)and energy due to the external loads (Ω) as follows (Reddy (2017)):

$$\Pi = U + \Omega \quad (17)$$

where

$$\begin{cases}U=\frac{1}{2}\int_{\forall}(\sigma_{xx}\varepsilon_{xx}+\sigma_{yy}\varepsilon_{yy}+\tau_{xy}\gamma_{xy}-D_xE_x-D_yE_y-D_zE_z)d\forall\\ \Omega=-\frac{1}{2}\int_0^b\int_0^a Fwdxdy\end{cases} \quad (18)$$

In which

$$F=N_{x_0}\left(\frac{\partial^2 w}{\partial x^2}\right)+N_{y_0}\left(\frac{\partial^2 w}{\partial y^2}\right)+q(x,y) \quad (19)$$

where $q(x,y)$ is transverse load per length and N_{x_0}, N_{y_0} are bi-axial forces.

The principle of minimum total potential energy:

The principle of minimum total potential energy is considered as:

$$\delta\Pi=0\Rightarrow\delta U+\delta\Omega=0 \quad (20)$$

where

$$\begin{cases}\delta U=\int_A\int_{-\frac{h}{2}}^{\frac{h}{2}}(\sigma_{xx}\delta\varepsilon_{xx}+\sigma_{yy}\delta\varepsilon_{yy}+\tau_{xy}\delta\gamma_{xy}-D_x\delta E_x-D_y\delta E_y-D_z\delta E_z)dzdA\\ \delta\Omega=-\int_0^b\int_0^a F\delta w dxdy\end{cases} \quad (21)$$

Given the following relationships (resultant forces and moments), the equations of equilibrium are obtained.

$$\begin{Bmatrix}N_x\\N_y\\N_{xy}\end{Bmatrix}=\int\begin{Bmatrix}\sigma_{xx}\\\sigma_{yy}\\\tau_{xy}\end{Bmatrix}dz \qquad \begin{Bmatrix}M_x\\M_y\\M_{xy}\end{Bmatrix}=\int\begin{Bmatrix}\sigma_{xx}\\\sigma_{yy}\\\tau_{xy}\end{Bmatrix}zdz \quad (22)$$

$$\begin{Bmatrix}\overline{D}_x\\\overline{D}_y\\\overline{D}_z\end{Bmatrix}=\int\begin{Bmatrix}D_x\\D_y\\D_z\end{Bmatrix}dz \quad (23)$$

By inserting equations (10-a), (13), (22) and (23) into Eq. (20) and finally, the four equations of equilibrium are obtained by separating the coefficients for each independent variable and zeroing the δu , δv , δw and $\delta\phi_E$ coefficients.

$$\delta u:\frac{\partial N_x}{\partial x}+\frac{\partial N_{xy}}{\partial y}=0 \quad (24)$$

$$\delta v:\frac{\partial N_y}{\partial y}+\frac{\partial N_{xy}}{\partial x}=0 \quad (25)$$

$$\delta w:\begin{cases}\dfrac{\partial^2 M_x}{\partial x^2}+\dfrac{\partial^2 M_y}{\partial y^2}+2\dfrac{\partial^2 M_{xy}}{\partial x\,\partial y}\\ +N_{x_0}\left(\dfrac{\partial^2 w}{\partial x^2}\right)+N_{y_0}\left(\dfrac{\partial^2 w}{\partial y^2}\right)+q(x,y)=0\end{cases} \quad (26)$$

$$\delta\phi_E:\frac{\partial\overline{D}_x}{\partial x}+\frac{\partial\overline{D}_y}{\partial y}+\frac{\partial\overline{D}_z}{\partial z}=0 \quad (27)$$

In order to complete the governing equations of equilibrium, first, by substituting strain-displacement equations (9) and electric-field equation (13) into the stress-strain equations (10-a), stress-displacement relations are obtained as shown in equation (28a). Also by substituting Eqs. (9) and (13) into Eq. (11), the electric displacement-electric field equation is obtained, which are stated in equation (28-b):

$$\begin{cases}\bullet\left(1-(ea)^2\nabla^2\right)\sigma_{xx}=\left(1-\ell^2\nabla^2\right)\begin{pmatrix}\frac{E_{x_{(z)}}}{1-\upsilon^2}\left(\frac{\partial u_0}{\partial x}-z\frac{\partial^2 w}{\partial x^2}+\frac{1}{2}(\frac{\partial w}{\partial x})^2\right)\\ +\frac{\upsilon E_{x_{(z)}}}{1-\upsilon^2}\left(\frac{\partial v_0}{\partial y}-z\frac{\partial^2 w}{\partial y^2}+\frac{1}{2}(\frac{\partial w}{\partial y})^2\right)\end{pmatrix}\\ -e_{31}\left(-\beta'\sin(\beta' z)\phi_E-\frac{2V_E}{h}\right)\\ \bullet\left(1-(ea)^2\nabla^2\right)\sigma_{yy}=\left(1-\ell^2\nabla^2\right)\begin{pmatrix}\frac{\upsilon E_{x_{(z)}}}{1-\upsilon}\left(\frac{\partial u_0}{\partial x}-z\frac{\partial^2 w}{\partial x^2}+\frac{1}{2}(\frac{\partial w}{\partial x})^2\right)\\ +\frac{E_{y_{(z)}}}{1-\upsilon^2}\left(\frac{\partial v_0}{\partial y}-z\frac{\partial^2 w}{\partial y^2}+\frac{1}{2}(\frac{\partial w}{\partial y})^2\right)\end{pmatrix}\\ -e_{32}\left(-\beta'\sin(\beta' z)\phi_E-\frac{2V_E}{h}\right)\\ \bullet\left(1-(ea)^2\nabla^2\right)\tau_{xy}=\left(1-\ell^2\nabla^2\right)E_{xy_{(z)}}\begin{pmatrix}\frac{\partial u_0}{\partial y}+\frac{\partial v_0}{\partial x}\\ -2z\frac{\partial^2 w}{\partial x\,\partial y}+(\frac{\partial w}{\partial x})(\frac{\partial w}{\partial y})\end{pmatrix}\end{cases} \quad (28\text{-a})$$

$$\begin{cases}\left(1-(ea)^2\nabla^2\right)D_x=\xi_{11}\left(\cos(\beta' z)\frac{\partial\phi_E}{\partial x}\right)\\ \left(1-(ea)^2\nabla^2\right)D_y=\xi_{22}\left(\cos(\beta' z)\frac{\partial\phi_E}{\partial y}\right)\\ \left(1-(ea)^2\nabla^2\right)D_Z=e_{31}\left(\frac{\partial u_0}{\partial x}-z\frac{\partial^2 w}{\partial x^2}+\frac{1}{2}(\frac{\partial w}{\partial x})^2\right)\\ +e_{32}\left(\frac{\partial v_0}{\partial y}-z\frac{\partial^2 w}{\partial y^2}+\frac{1}{2}(\frac{\partial w}{\partial y})^2\right)+\xi_{33}\left(-\beta'\sin(\beta' z)\phi_E-\frac{2V_E}{h}\right)\end{cases} \quad (28\text{-b})$$

By employing the equations of Appendix A into equations (28-a, 28-b) and replacing them into equation (22), the resultant forces and moments are obtained which are given in Appendix B.

Finally, the governing equations of equilibrium are completed by substituting the equations of Appendix B into equations (24) to (27).

5. Analytical solutions

In this paper, Navier's type solution is employed to consider the static solutions of a simply supported rectangular plate subjected to a transverse load $(q(x,y))$ and bi-axial forces $\left(N_{x_0}=\gamma_1 N_{cr}\ ,\ N_{y_0}=\gamma_2 N_{cr}\right.$ and $\left.N_{xy_0}=0\right)$. Based on this method, in order to satisfy the equations of equilibrium and boundary conditions, the solution is considered as the following relations (Thai and Choi (2013), Reddy (2017)):

$$\begin{cases} u(x,y)=\sum_{m=1}^{\infty}\sum_{n=1}^{\infty}U_{mn}\cos\alpha x\,\sin\beta y \\ v(x,y)=\sum_{m=1}^{\infty}\sum_{n=1}^{\infty}V_{mn}\sin\alpha x\,\cos\beta y \\ w(x,y)=\sum_{m=1}^{\infty}\sum_{n=1}^{\infty}W_{mn}\sin\alpha x\,\sin\beta y \\ \phi_E(x,y)=\sum_{m=1}^{\infty}\sum_{n=1}^{\infty}\Phi_{mn}\sin\alpha x\,\sin\beta y \\ q(x,y)=\sum_{m=1}^{\infty}\sum_{n=1}^{\infty}Q_{mn}\sin\alpha x\,\sin\beta y \end{cases} \tag{29}$$

where $\alpha=\frac{m\pi}{a}$, $\beta=\frac{m\pi}{b}$, $\{U_{mn},V_{mn},W_{mn},\Phi_{mn}\}$ are coefficients and Q_{mn} is obtained by following equation (Reddy (2017)):

$$Q_{mn}=\frac{4}{ab}\int_0^a\int_0^b q(x,y)\sin\alpha x\,\sin\beta y dxdy \tag{30}$$

Three various cases for transverse load $(q(x,y))$ are considered as follows:

$$q(x,y)=\begin{cases} q_0\sin\alpha_1 x\,\sin\beta_1 y & \text{sinusoidal load of intensity } q_0 \quad \text{(case a)},\ \alpha_1=\frac{i\pi}{a},\beta_1=\frac{j\pi}{b} \\ q_0 & \text{uniform load of intensity } q_0 \quad \text{(case b)} \\ Q_0\ \delta(x-\frac{a}{2})\,\delta(y-\frac{b}{2}) & \text{point load } Q_0 \text{ at the center} \quad \text{(case c)} \end{cases} \tag{31-a}$$

Also, by substituting Eqs. (31) into Eq. (30), Q_{mn} varies for different loading as follows (Reddy (2017)):

$$Q_{mn}=\begin{cases} q_0 & \text{sinusoidal load of intensity } q_0 \quad \text{(case a)} \\ \frac{16q_0}{mn\pi^2} & \text{uniform load of intensity } q_0 \quad \text{(case b)} \\ \frac{4Q_0}{ab}\sin\frac{m\pi}{2}\sin\frac{n\pi}{2} & \text{point load } Q_0 \text{ at the center} \quad \text{(case c)} \end{cases} \tag{31-b}$$

By substituting equation (29) into equations of equilibrium, the equations of CPT for buckling and bending can be obtained as follows:

For buckling analysis:

$$\frac{\partial^2 M_x}{\partial x^2}+\frac{\partial^2 M_y}{\partial y^2}+2\frac{\partial^2 M_{xy}}{\partial x\partial y}=N_{x_0}\left(\frac{\partial^2 w}{\partial x^2}\right)+N_{y_0}\left(\frac{\partial^2 w}{\partial y^2}\right) \tag{32-a}$$

$$\begin{aligned} N_{x_0}&=\gamma_1 N_{cr} \\ N_{y_0}&=\gamma_2 N_{cr} \end{aligned} \tag{32-b}$$

Equation (32-a) is a static buckling equation which is used for obtaining the critical buckling load. M_x, M_y and M_{xy} are the resultant moments and obtained by equation (22). N_{x_0} and N_{y_0} are the resultant bi-axial forces and calculated by equation (32-b) to obtain the critical buckling load (N_{cr}).

For bending analysis:

$$\begin{bmatrix} k_{11} & k_{12} & k_{13} & k_{14} \\ k_{21} & k_{22} & k_{23} & k_{24} \\ k_{31} & k_{32} & k_{33} & k_{34} \\ k_{41} & k_{42} & k_{43} & k_{44} \end{bmatrix}\begin{Bmatrix} U_{mn} \\ V_{mn} \\ W_{mn} \\ \Phi_{mn} \end{Bmatrix}=\begin{Bmatrix} 0 \\ 0 \\ Q_{mn} \\ 0 \end{Bmatrix} \tag{33}$$

where the elements of stiffness matrix [K] are given in equations (34-a to 34-m).

$$k_{11}=\begin{pmatrix} A_x^0\left(\frac{1}{1-\upsilon^2}\right)\begin{pmatrix} -\alpha^2-\ell^2(\alpha^4+\alpha^2\beta^2) \\ +(ea)^2\begin{pmatrix} \alpha^4-\ell^2(-\alpha^6-\alpha^4\beta^2) \\ +\alpha^2\beta^2-\ell^2(-\alpha^4\beta^2-\alpha^2\beta^4) \end{pmatrix} \end{pmatrix} \\ +A_{xy}^0\begin{pmatrix} -\beta^2-\ell^2(\alpha^2\beta^2+\beta^4) \\ +(ea)^2\begin{pmatrix} \alpha^2\beta^2-\ell^2(-\alpha^4\beta^2-\alpha^2\beta^4) \\ +\beta^4-\ell^2(-\alpha^2\beta^4-\beta^6) \end{pmatrix} \end{pmatrix} \end{pmatrix} \tag{34-a}$$

$$k_{12}=\begin{pmatrix} A_x^0\left(\frac{\upsilon}{1-\upsilon^2}\right)\begin{pmatrix} -\alpha\beta-\ell^2(\alpha^3\beta+\alpha\beta^3) \\ +(ea)^2\begin{pmatrix} \alpha^3\beta-\ell^2(-\alpha^5\beta-\alpha^3\beta^3) \\ +\alpha\beta^3-\ell^2(-\alpha^3\beta^3-\alpha\beta^5) \end{pmatrix} \end{pmatrix} \\ +A_{xy}^0\begin{pmatrix} -\alpha\beta-\ell^2(\alpha^3\beta+\alpha\beta^3) \\ +(ea)^2\begin{pmatrix} \alpha^3\beta-\ell^2(-\alpha^5\beta-\alpha^3\beta^3) \\ +\alpha\beta^3-\ell^2(-\alpha^3\beta^3-\alpha\beta^5) \end{pmatrix} \end{pmatrix} \end{pmatrix} \tag{34-b}$$

$$k_{13}=\begin{pmatrix} A_x^1\left(\frac{1}{1-\upsilon^2}\right)\begin{pmatrix}\alpha^3+\upsilon\alpha\beta^2-\prime^2(-\alpha^5-\upsilon\alpha^3\beta^2-\alpha^3\beta^2-\upsilon\alpha\beta^4)\\ +(ea)^2\begin{pmatrix}-\alpha^5-\upsilon\alpha^3\beta^2-\prime^2(\alpha^7+\upsilon\alpha^5\beta^2+\alpha^5\beta^2+\upsilon\alpha^3\beta^4)\\ -\alpha^3\beta^2-\upsilon\alpha\beta^4-\prime^2(\alpha^5\beta^2+\upsilon\alpha^3\beta^4+\alpha^3\beta^4+\upsilon\alpha\beta^6)\end{pmatrix}\end{pmatrix}\\ +2A_{xy}^1\left(\alpha\beta^2-\prime^2(-\alpha^3\beta^2-\alpha\beta^4)+(ea)^2\begin{pmatrix}-\alpha^3\beta^2-\prime^2(\alpha^5\beta^2+\alpha^3\beta^4)\\ -\alpha\beta^4-\prime^2(\alpha^3\beta^4+\alpha\beta^6)\end{pmatrix}\right)\end{pmatrix} \tag{34-c}$$

$$k_{14}=C^0e_{31}\beta'\alpha-((ea)^2)C^0e_{31}\beta 1(\alpha^3+\alpha\beta^2) \tag{34-d}$$

$$k_{21}=\begin{pmatrix} A_x^0\left(\frac{\upsilon}{1-\upsilon^2}\right)\left(-\alpha\beta-\prime^2(\alpha^3\beta+\alpha\beta^3)+(ea)^2\begin{pmatrix}\alpha^3\beta-\prime^2(-\alpha^5\beta-\alpha^3\beta^3)\\ +\alpha\beta^3-\prime^2(-\alpha^3\beta^3-\alpha\beta^5)\end{pmatrix}\right)\\ +A_{xy}^0\left(-\alpha\beta-\prime^2(\alpha^3\beta+\alpha\beta^3)+(ea)^2\begin{pmatrix}\alpha^3\beta-\prime^2(-\alpha^5\beta-\alpha^3\beta^3)\\ +\alpha\beta^3-\prime^2(-\alpha^3\beta^3-\alpha\beta^5)\end{pmatrix}\right)\end{pmatrix} \tag{34-e}$$

$$k_{22}=\begin{pmatrix} A_y^0\left(\frac{1}{1-\upsilon^2}\left(-\beta^2-\prime^2(\beta^4+\alpha^2\beta^2)+(ea)^2\begin{pmatrix}\alpha^2\beta^2-\prime^2(-\alpha^2\beta^4-\alpha^4\beta^2)\\ +\beta^4-\prime^2(-\beta^6-\alpha^2\beta^4)\end{pmatrix}\right)\right)\\ +A_{xy}^0\left(-\alpha^2-\prime^2(\alpha^2\beta^2+\alpha^4)+(ea)^2\begin{pmatrix}\alpha^4-\prime^2(-\alpha\beta^2-\alpha^6)\\ +\alpha^2\beta^2-\prime^2(-\alpha^2\beta^4-\alpha^4\beta^2)\end{pmatrix}\right)\end{pmatrix} \tag{34-f}$$

$$k_{23}=\begin{pmatrix} A_x^1\left(\frac{\upsilon}{1-\upsilon^2}\right)\left(\alpha^2\beta-\prime^2(-\alpha^4\beta-\alpha^2\beta^3)+(ea)^2\begin{pmatrix}-\alpha^4\beta-\prime^2(\alpha^6\beta+\alpha^4\beta^3)\\ -\alpha^2\beta^3-\prime^2(\alpha^4\beta^3+\alpha^2\beta^5)\end{pmatrix}\right)\\ +A_y^1\frac{1}{1-\upsilon^2}\left(\beta^3-\prime^2(-\beta^5-\alpha^2\beta^3)+(ea)^2\begin{pmatrix}-\alpha^2\beta^3-\prime^2(\alpha^4\beta^3+\alpha^2\beta^5)\\ -\beta^5-\prime^2(\alpha^2\beta^5+\beta^7)\end{pmatrix}\right)\\ +2A_{xy}^1\left(\alpha^2\beta-(\prime^2)(-\alpha^4\beta-\alpha^2\beta^3)+(ea)^2\begin{pmatrix}-\alpha^4\beta-\prime^2(\alpha^6\beta+\alpha^4\beta^3)\\ -\alpha^2\beta^3-\prime^2(\alpha^4\beta^3+\alpha^2\beta^5)\end{pmatrix}\right)\end{pmatrix} \tag{34-g}$$

$$k_{24}=C^0e_{32}\beta'\beta-(ea)^2C^0e_{32}\beta_1(\beta^3+\alpha^2\beta) \tag{34-h}$$

$$k_{31}=\begin{pmatrix} A_x^1\left(\frac{1}{1-\upsilon^2}\right)\begin{pmatrix}\alpha^3+\upsilon\alpha\beta^2-\prime^2(-\alpha^5-\upsilon\alpha^3\beta^2-\alpha^3\beta^2-\upsilon\alpha\beta^4)\\ +(ea)^2\begin{pmatrix}-\alpha^5-\upsilon\alpha^3\beta^2-\prime^2(\alpha^7+\upsilon\alpha^5\beta^2+\alpha^5\beta^2+\upsilon\alpha^3\beta^4)\\ -\alpha^3\beta^2-\upsilon\alpha\beta^4-\prime^2(\alpha^5\beta^2+\upsilon\alpha^3\beta^4+\alpha^3\beta^4+\upsilon\alpha\beta^6)\end{pmatrix}\end{pmatrix}\\ +2A_{xy}^1\left(\alpha\beta^2-\prime^2(-\alpha^3\beta^2-\alpha\beta^4)+(ea)^2\begin{pmatrix}-\alpha^3\beta^2-\prime^2(\alpha^5\beta^2+\alpha^3\beta^4)\\ -\alpha\beta^4-\prime^2(\alpha^3\beta^4+\alpha\beta^6)\end{pmatrix}\right)\end{pmatrix} \tag{34-i}$$

$$k_{32}=\begin{pmatrix} A_x^1\left(\frac{\upsilon}{1-\upsilon^2}\right)\left(\alpha^2\beta-\prime^2(-\alpha^4\beta-\alpha^2\beta^3)+(ea)^2\begin{pmatrix}-\alpha^4\beta-\prime^2(\alpha^6\beta+\alpha^4\beta^3)\\ -\alpha^2\beta^3-\prime^2(\alpha^4\beta^3+\alpha^2\beta^5)\end{pmatrix}\right)\\ +A_y^1\frac{1}{1-\upsilon^2}\left(\beta^3-\prime^2(-\beta^5-\alpha^2\beta^3)+(ea)^2\begin{pmatrix}-\alpha^2\beta^3-\prime^2(\alpha^4\beta^3+\alpha^2\beta^5)\\ -\beta^5-\prime^2(\alpha^2\beta^5+\beta^7)\end{pmatrix}\right)\\ +2A_{xy}^1\left(\alpha^2\beta-(\prime^2)(-\alpha^4\beta-\alpha^2\beta^3)+(ea)^2\begin{pmatrix}-\alpha^4\beta-\prime^2(\alpha^6\beta+\alpha^4\beta^3)\\ -\alpha^2\beta^3-\prime^2(\alpha^4\beta^3+\alpha^2\beta^5)\end{pmatrix}\right)\end{pmatrix} \tag{34-j}$$

$$k_{33}=\begin{pmatrix} A_x^2\frac{1}{1-\upsilon^2}\begin{pmatrix} -\alpha^4-\upsilon\alpha^2\beta^2-i^2(\alpha^6+\upsilon\alpha^4\beta^2+\alpha^4\beta^2+\upsilon\alpha^2\beta^4) \\ +(ea)^2\begin{pmatrix} \alpha^6+\upsilon\alpha^4\beta^2-i^2\begin{pmatrix}-\alpha^8-\upsilon\alpha^6\beta^2\\ -\alpha^6\beta^2-\upsilon\alpha^4\beta^4\end{pmatrix} \\ +\alpha^4\beta^2+\upsilon\alpha^2\beta^4-i^2\begin{pmatrix}-\alpha^6\beta^2-\upsilon\alpha^4\beta^4\\ -\alpha^4\beta^4-\upsilon\alpha^2\beta^6\end{pmatrix}\end{pmatrix}\end{pmatrix} \\ +\frac{1}{1-\upsilon^2}\begin{pmatrix} -A_y^2\beta^4-A_x^2\upsilon\alpha^2\beta^2-i^2\begin{pmatrix}A_y^2\alpha^2\beta^4+A_x^2\upsilon\alpha^4\beta^2\\ +A_y^2\beta^6+A_x^2\upsilon\alpha^2\beta^4\end{pmatrix} \\ +(ea)^2\begin{pmatrix} A_y^2\alpha^2\beta^4+A_x^2\upsilon\alpha^4\beta^2-i^2\begin{pmatrix}-A_y^2\alpha^4\beta^4-A_x^2\upsilon\alpha^6\beta^2\\ -A_y^2\alpha^2\beta^6-A_x^2\upsilon\alpha^4\beta^4\end{pmatrix} \\ +A_y^2\beta^6+A_x^2\upsilon\alpha^2\beta^4-i^2\begin{pmatrix}-A_y^2\alpha^2\beta^6-A_x^2\upsilon\alpha^4\beta^4\\ -A_y^2\beta^8-A_x^2\upsilon\alpha^2\beta^6\end{pmatrix}\end{pmatrix}\end{pmatrix} \\ +4A_{xy}^2\begin{pmatrix}-\alpha^2\beta^2-i^2(\alpha^4\beta^2+\alpha^2\beta^4)\\ +(ea)^2\begin{pmatrix}\alpha^4\beta^2-i^2(-\alpha^4\beta^4-\alpha^6\beta^2)\\ +\alpha^2\beta^4-i^2(-\alpha^4\beta^4-\alpha^2\beta^6)\end{pmatrix}\end{pmatrix} \end{pmatrix} \tag{34-k}$$

$$k_{34}=C^1e_{31}\beta'(-\alpha^2+(ea)^2(\alpha^4+\alpha^2\beta^2))+C^1e_{32}\beta'(-\beta^2+(ea)^2(\beta^4+\alpha^2\beta^2)) \tag{34-l}$$

$$\begin{aligned} k_{41}&=0\\ k_{42}&=0\\ k_{43}&=0\\ k_{44}&=d_{11}D^0(-\alpha^2+(ea)^2(\alpha^4+\alpha^2\beta^2))+d_{22}D^0(-\beta^2+(ea)^2(\beta^4+\alpha^2\beta^2)) \end{aligned} \tag{34-m}$$

6. Numerical results and discussion

To study the validity of this procedure, since the results of FG-SWCNTs-reinforced microplate are not available in this literature, the porosity coefficient is considered zero (homogeneous plate ($e_0=0$)). Table 5 summarizes the analogy of non-dimensional deflection and critical buckling load for a homogenous simply supported square plate with various values of aspect ratio (a/h). This comparison is done with those reported by Thai and Choi (2013) based on Kirchhoff plate theory (KPT). With this comparison, it can be observed that results of the present work are consistent with the results of Thai and Choi (2013). In this comparison, the following equation for asymmetric porous material are considered (Magnucka-Blandzi (2008), Thai and Choi (2013)):

$$\begin{cases} E_{(z)}=E_0\left(1\text{-}e_0\cos\left(\frac{\pi}{2h}(z+\frac{h}{2})\right)\right) \\ \rho_{(z)}=\rho_0\left(1\text{-}e_0'\cos\left(\frac{\pi}{2h}(z+\frac{h}{2})\right)\right) \\ e_0'=1-\sqrt{1-e_0} \end{cases} \tag{35}$$

$$\begin{cases} E_0=14.4Gpa & e_0=0 & a=b & t=0 \\ E_1=1.44Gpa & q_0=1N & h=17.6\times10^{-6}m & \\ \rho_0=12200\,Kg/m^3 & \rho_1=1220\,Kg/m^3 & \nu=0.38 & \end{cases} \tag{36}$$

In Eq. (35), it is assumed that the distribution of porous material becomes as asymmetric distribution.

Since this case isn't piezoelectric, the analytical solutions of the CPT can be obtained from the following equation (Reddy (2017)):

$$\begin{bmatrix} k_{11} & k_{12} & k_{13} \\ k_{21} & k_{22} & k_{23} \\ k_{31} & k_{32} & k_{33} \end{bmatrix}\begin{Bmatrix} U_{mn} \\ V_{mn} \\ W_{mn} \end{Bmatrix}=\begin{Bmatrix} 0 \\ 0 \\ Q_{mn} \end{Bmatrix} \tag{37}$$

The nondimensional deflection $\overline{W}$ and critical buckling load $\overline{N}$ are acquired from following equations (Thai and Choi (2013)):

$$\begin{aligned} \overline{W}&=\frac{100E_1h^3}{q_0a^4}W\left(\frac{a}{2},\frac{b}{2}\right)\\ \overline{N}&=\frac{N_{cr}a^2}{E_1h^3} \end{aligned} \tag{38}$$

Table 5 Comparison of nondimensional deflection and critical buckling load of a homogenous simply supported square plate with various values of aspect ratio

$\overline{W}$	a/h	Thai and Choi (2013)	Present work	Diff (%)
For uniform load $\left(Qmn=\frac{16q_0}{mn\pi^2}\right)$	5	0.4171	0.4272	2.4214
	10	0.4171	0.4272	2.4214
	20	0.4171	0.4272	2.4214
For sinusoidal load $(Qmn=q_0)$	5	0.2635	0.2635	0
	10	0.2635	0.2635	0
	20	0.2635	0.2635	0
$\overline{N}$	a/h	Thai and Choi (2013)	Present work	Diff (%)
For biaxial buckling $(\gamma_1=\gamma_2=-1)$	5	19.2255	19.2255	0
	10	19.2255	19.2255	0
	20	19.2255	19.2255	0
For uniaxial buckling $(\gamma_1=-1,\gamma_2=0)$	5	38.4510	38.4510	0
	10	38.4510	38.4510	0
	20	38.4510	38.4510	0

where W and N_{cr} are the deflection and critical buckling load, respectively.

Assume a simply supported square FG-SWCNTs-reinforced plate with the following material properties:

$$\begin{cases} h=340\ nm & T=300\ K \\ ea=0.5\ nm & \Delta T=25 \\ V_{CNT}=0.11 & e_0=0,0.2,0.5,0.9 \\ a=b & q_0=1000\ N \end{cases} \tag{39}$$

6.1 Bending analysis of the FG-SWCNTs-reinforced porous nanocomposite piezoelectric rectangular plate

In Table 6, deflections caused by uniform and sinusoidal loadings of the porous nanocomposite piezoelectric plate reinforced by CNT are listed with various values of porosity coefficient for different material length scale parameter and aspect ratio values. It is observed that with increasing porosity coefficient and aspect ratio, deflection increases and by increasing material length scale parameter, the deflection of CPT decreases.

To indicate the effect of porosity coefficient on the deflection of a FG-SWCNTs-reinforced porous nanocomposite piezoelectric plate, Figs. 3 and 4 plot the dimensional and nondimensional deflection with respect to aspect ratio *a*/*h* for a simply supported square plate, respectively. Figures 3 and 4 illustrate that as aspect ratio and porosity coefficient increase, the dimensional and nondimensional deflection of CPT increase however nondimensional deflection limits to a constant value by increasing aspect ratio. In the other words, by increasing porosity coefficient, the stiffness of the plate decreases and as a result deflection increases.

Table 6 Deflection W (10^{-9} m) of a simply supported FG-SWCNTs-reinforced plate with various values of porosity coefficient

Uniform load $\left(Qmn=\frac{16q_0}{mn\pi^2}\right)$ a/h	ℓ/h	$e_0=0$	$e_0=0.2$	$e_0=0.5$	$e_0=0.9$
10	0	0.0049	0.0056	0.0073	0.0161
	0.2	0.0048	0.0055	0.0072	0.0160
	0.5	0.0047	0.0053	0.0069	0.0154
	0.8	0.0043	0.0049	0.0064	0.0143
	1	0.0041	0.0047	0.0061	0.0134
20	0	0.0787	0.0894	0.1163	0.2580
	0.2	0.0785	0.0892	0.1161	0.2575
	0.5	0.0777	0.0883	0.1149	0.2548
	0.8	0.0763	0.0867	0.1128	0.2501
	1	0.0750	0.0852	0.1109	0.2458
30	0	0.3983	0.4527	0.5889	1.3060
	0.2	0.3979	0.4523	0.5884	1.3049
	0.5	0.3961	0.4503	0.5857	1.2989
	0.8	0.3927	0.4465	0.5808	1.2879
	1	0.3897	0.4430	0.5763	1.2780
40	0	1.2587	1.4309	1.8614	4.1278
	0.2	1.2581	1.4302	1.8605	4.1257
	0.5	1.2548	1.4265	1.8557	4.1151
	0.8	1.2488	1.4197	1.8468	4.0954
	1	1.2433	1.4134	1.8387	4.0774
Sinusoidal load $(Qmn=q_0)$ a/h	ℓ/h	$e_0=0$	$e_0=0.2$	$e_0=0.5$	$e_0=0.9$
10	0	0.0030	0.0034	0.0044	0.0099
	0.2	0.0030	0.0034	0.0044	0.0099
	0.5	0.0029	0.0033	0.0043	0.0095
	0.8	0.0027	0.0031	0.0040	0.0088
	1	0.0025	0.0029	0.0037	0.0083
20	0	0.0485	0.0552	0.0717	0.1591
	0.2	0.0484	0.0550	0.0716	0.1588
	0.5	0.0479	0.0545	0.0709	0.1572
	0.8	0.0470	0.0535	0.0696	0.1543
	1	0.0462	0.0526	0.0684	0.1516
30	0	0.2457	0.2793	0.3633	0.8057
	0.2	0.2454	0.2790	0.3630	0.8049
	0.5	0.2443	0.2777	0.3613	0.8012
	0.8	0.2423	0.2754	0.3582	0.7945
	1	0.2404	0.2733	0.3555	0.7883
40	0	0.7764	0.8827	1.1481	2.5462
	0.2	0.7760	0.8822	1.1476	2.5449
	0.5	0.7740	0.8799	1.1447	2.5384
	0.8	0.7703	0.8757	1.1392	2.5262
	1	0.7670	0.8719	1.1346	2.5153

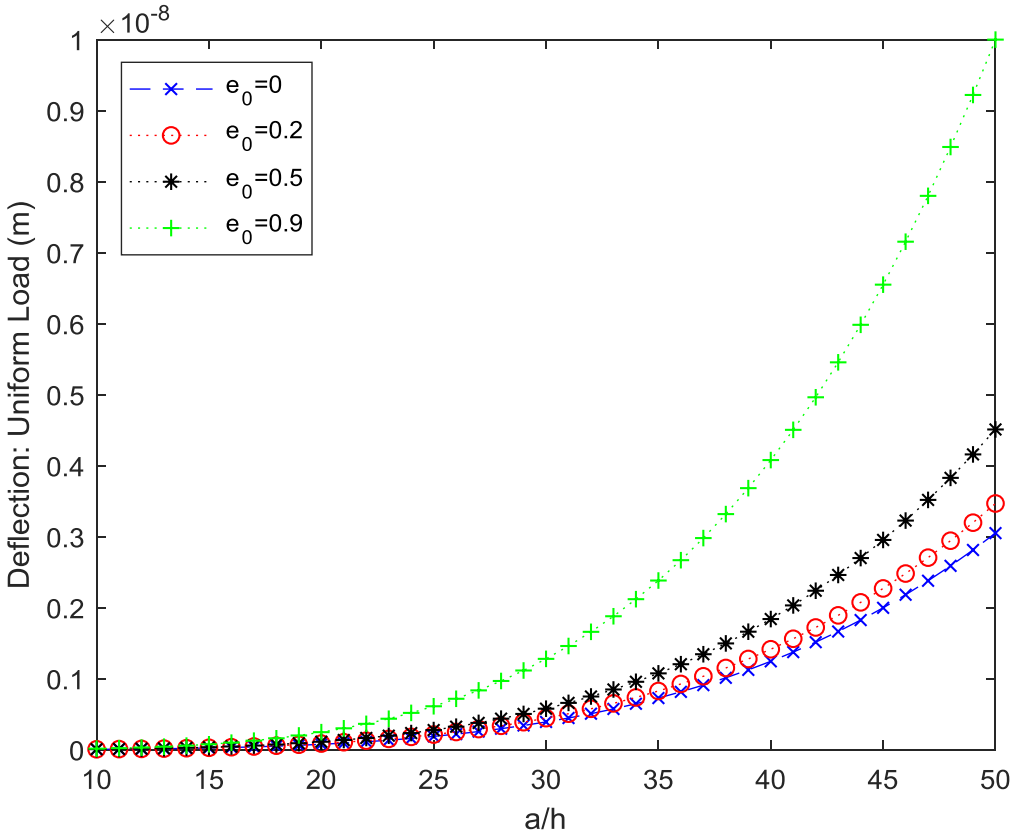

(a)

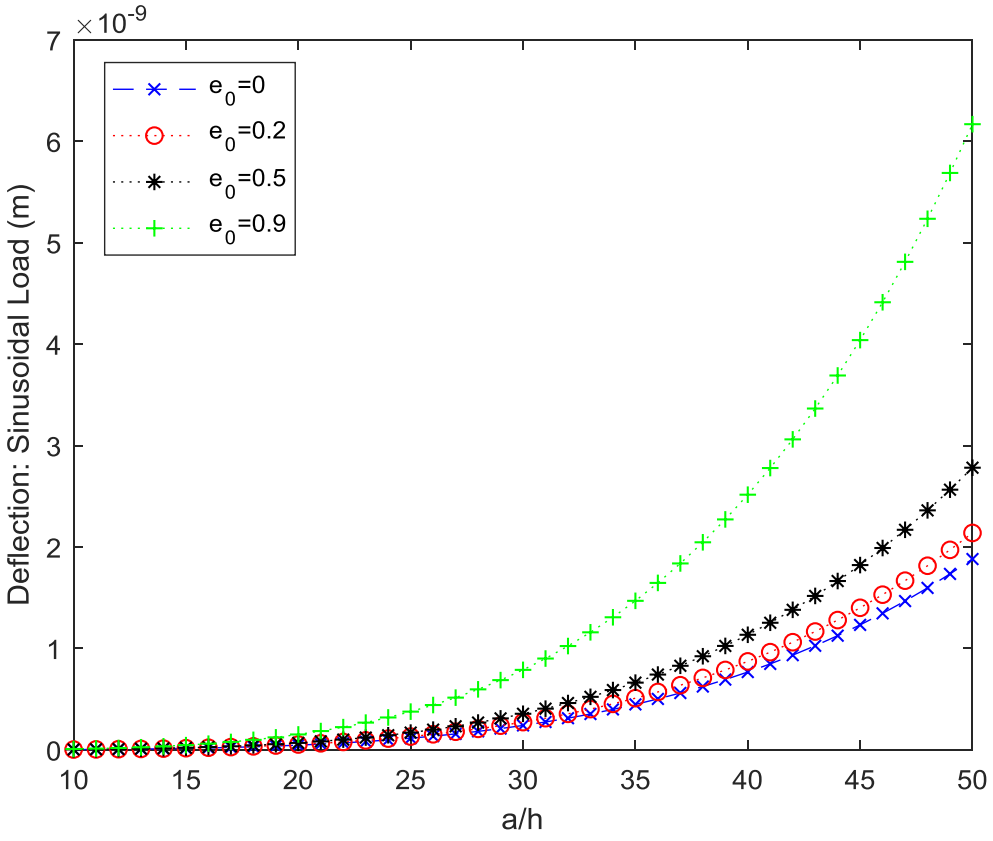

(b)

Fig. 3 Effect of porosity coefficient on the deflection of a simply supported FG-SWCNTs-reinforced plate: (a) under uniform loading (b) under sinusoidal loading

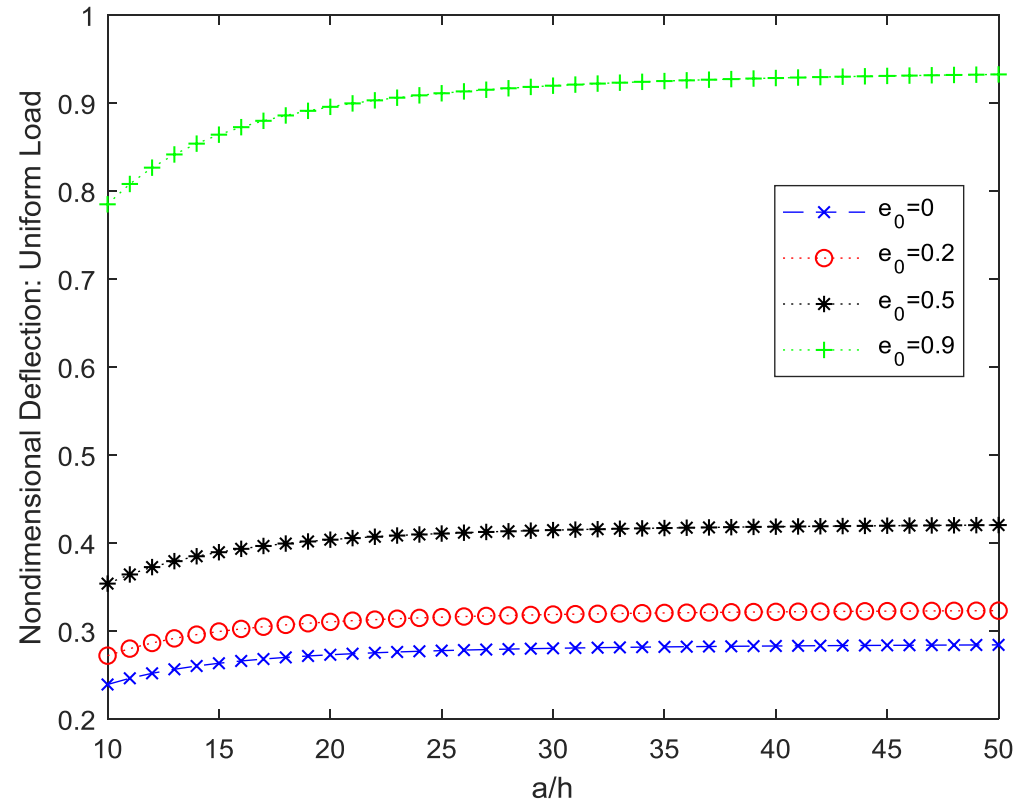

(a)

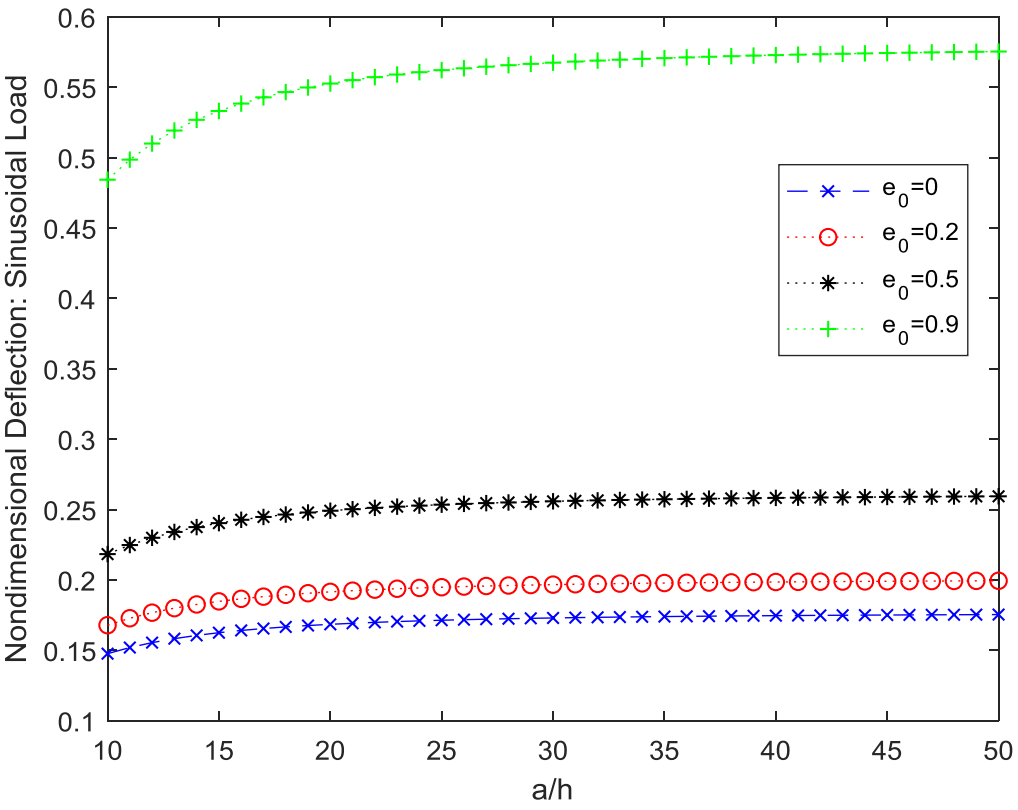

(b)

Fig. 4 Effect of porosity coefficient on the nondimensional deflection of a simply supported FG-SWCNTs-reinforced plate: (a) under uniform loading (b) under sinusoidal loading

Table 7 Deflection W (10^{-12} m) of a simply supported FG-SWCNTs-reinforced plate with various values Eringen's nonlocal parameter with $h = 20$ nm and $e_0 = 0.5$

Uniform load $\left(Qmn = \frac{16q_0}{mn\pi^2}\right)$ a/h	t/h	$ea = 0$	$ea = 0.5\ nm$	$ea = 1\ nm$	$ea = 1.5\ nm$	$ea = 2\ nm$
	0	0.4277	0.4278	0.4279	0.4282	0.4285
10	0.5	0.4076	0.4076	0.4078	0.4080	0.4084
	1	0.3572	0.3572	0.3574	0.3576	0.3579
	0	6.8433	6.8435	6.8441	6.8452	6.8467
20	0.5	6.7599	6.7601	6.7608	6.7618	6.7633
	1	6.5215	6.5217	6.5223	6.5223	6.5247
	0	34.6444	34.6449	34.6463	34.6487	34.6520
30	0.5	34.4555	34.4559	34.4574	34.4597	34.4630
	1	33.9009	33.9013	33.9027	33.9050	33.9083
	0	109.4934	109.4942	109.4968	109.5010	109.5069
40	0.5	109.1567	109.1576	109.1601	109.1643	109.7021
	1	108.1590	108.1599	108.1623	108.1665	108.1724
Sinusoidal load $(Qmn = q_0)$ a/h	t/h	$ea = 0$	$ea = 0.5\ nm$	$ea = 1\ nm$	$ea = 1.5\ nm$	$ea = 2\ nm$
	0	0.2638	0.2639	0.2640	0.2641	0.2643
10	0.5	0.2514	0.2514	0.2515	0.2517	0.2519
	1	0.2203	0.2204	0.2204	0.2206	0.2208
	0	4.2213	4.2214	4.2218	4.2225	4.2234
20	0.5	4.1699	4.1699	4.1704	4.1710	4.1719
	1	4.0228	4.0229	4.0233	4.0239	4.0248
	0	21.3704	21.3707	21.3716	21.3730	21.3751
30	0.5	21.2539	21.2542	21.2550	21.2565	21.2585
	1	20.9117	20.9120	20.9129	20.9143	20.9163
	0	67.5410	67.5415	67.5431	67.5457	67.5494
40	0.5	67.3333	67.3338	67.3354	67.3380	67.3417
	1	66.7179	66.7184	66.7200	66.7225	66.7262

To demonstrate the effect of Eringen's nonlocal parameter on the deflection of the porous nanocomposite piezoelectric plate reinforced by FG-SWCNTs, see Table 7. In this Table, deflections caused by uniform and sinusoidal loadings are presented with various values of Eringen's nonlocal parameter, material length scale parameter and aspect ratio values. It can be observed that with increasing Eringen's nonlocal parameter and aspect ratio, the deflection of CPT increases and by increasing length scale parameter, it is vice versa.

Figures 3 to 5 show that deflection caused by uniform loading is more than the other case with sinusoidal loading. Figure 5 (a) illustrates the effect of Eringen's nonlocal parameter on the deflection (uniform and sinusoidal loading) of a simply supported square plate reinforced by FG-SWCNTs with $h = 20$ nm, and $e_0 = 0.5$. Figure 5 (b) shows that the deflection of CPT increases by increasing of the Eringen's nonlocal parameter.

It can be seen from Fig. 6 that the effect of porosity coefficient on the increase of the deflection is greatly higher than the other parameters effect, and the Eringen's nonlocal parameter and the material length scale parameter have a lower effect on the deflection increase than the porosity coefficient, respectively.

6.2 Buckling analysis of the FG-SWCNTs-reinforced porous nanocomposite piezoelectric rectangular plate

In Table 8, critical buckling load caused by biaxial and uniaxial buckling loads of the porous nanocomposite piezoelectric plate are tabulated with various values of porosity coefficient, material length scale parameter and aspect ratio. It is observed that with increasing of porosity coefficient, and material length scale parameter, the deflection of CPT increases and by increasing aspect ratio, deflection decreases with the exception for $e_0 = 0.2$.

The effect of porosity coefficient with respect to aspect ratio a/h on the dimensional and nondimensional critical buckling load of a simply supported FG-SWCNTs-

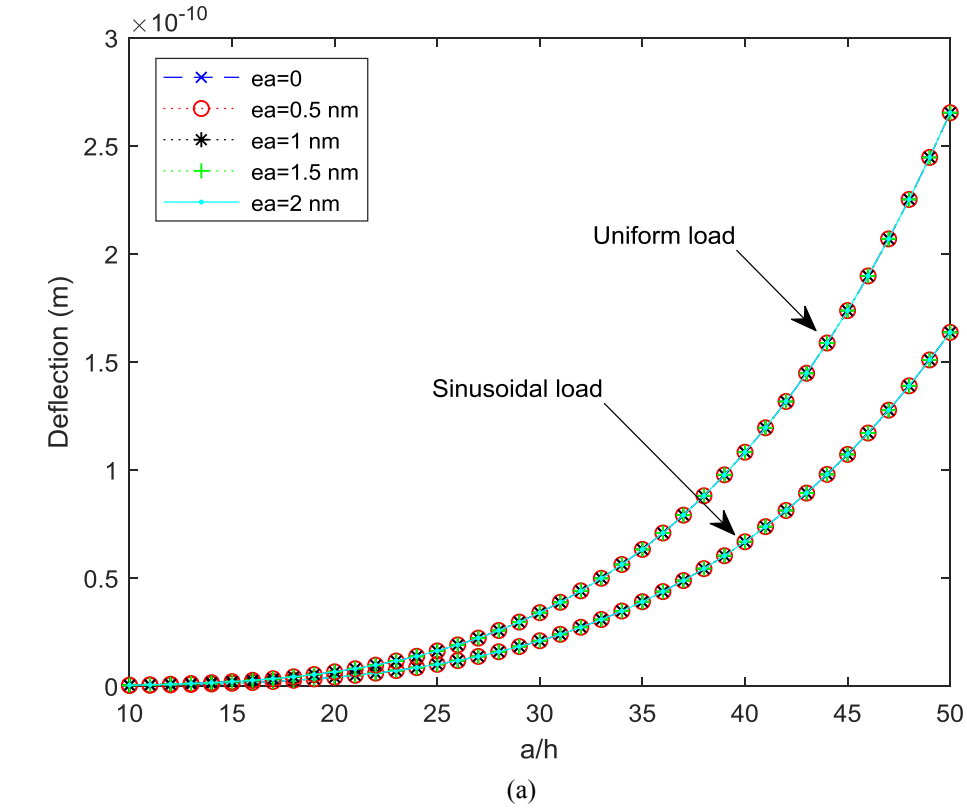

(a)

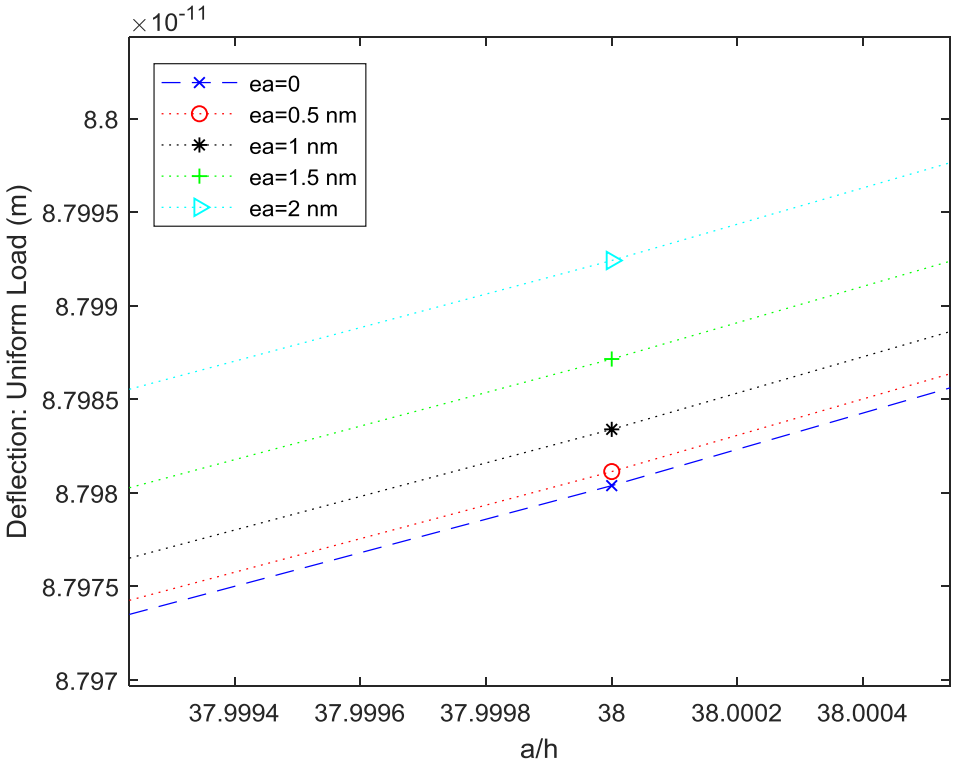

(b)

Fig. 5 Effect of Eringen's nonlocal parameter on the deflection of a simply supported FG-SWCNTs-reinforced plate with $h = 20$ nm, and $e_0 = 0.5$: (a) under uniform and sinusoidal loading (b) under uniform loading

reinforced plate is shown in Figures 7 and 8, respectively. It is also depicted from these figures, as porosity coefficient increases, dimensional and nondimensional critical buckling load increase. But by increasing of the value of aspect ratio, dimensional critical buckling load decreases and vice versa for nondimensional critical buckling load.

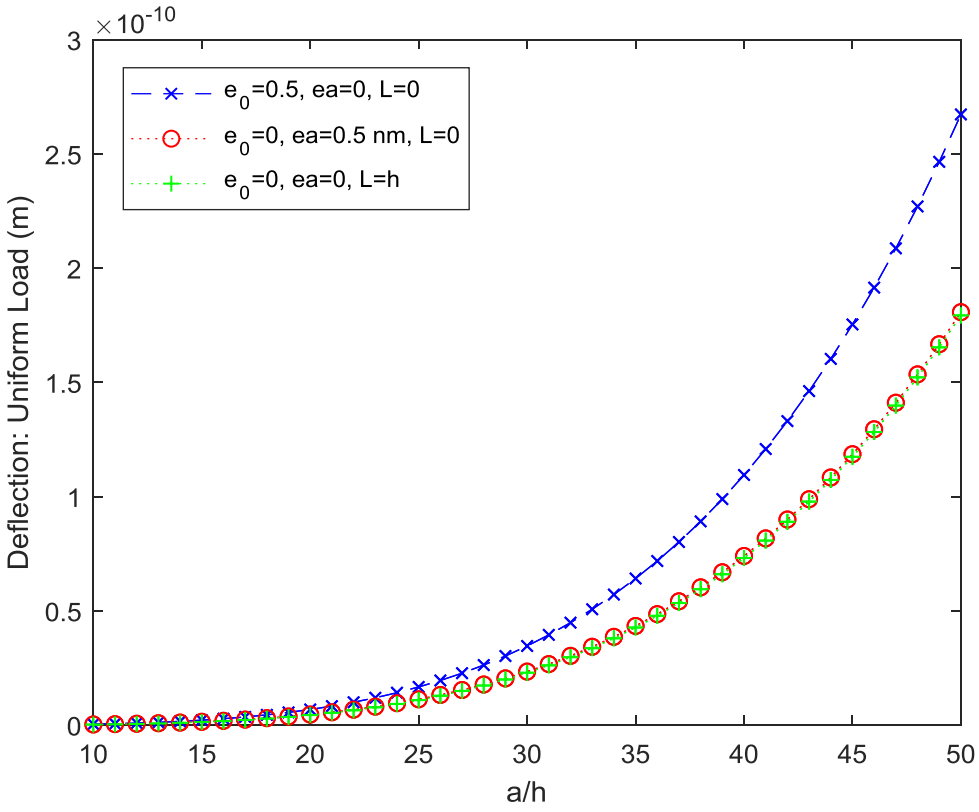

(a)

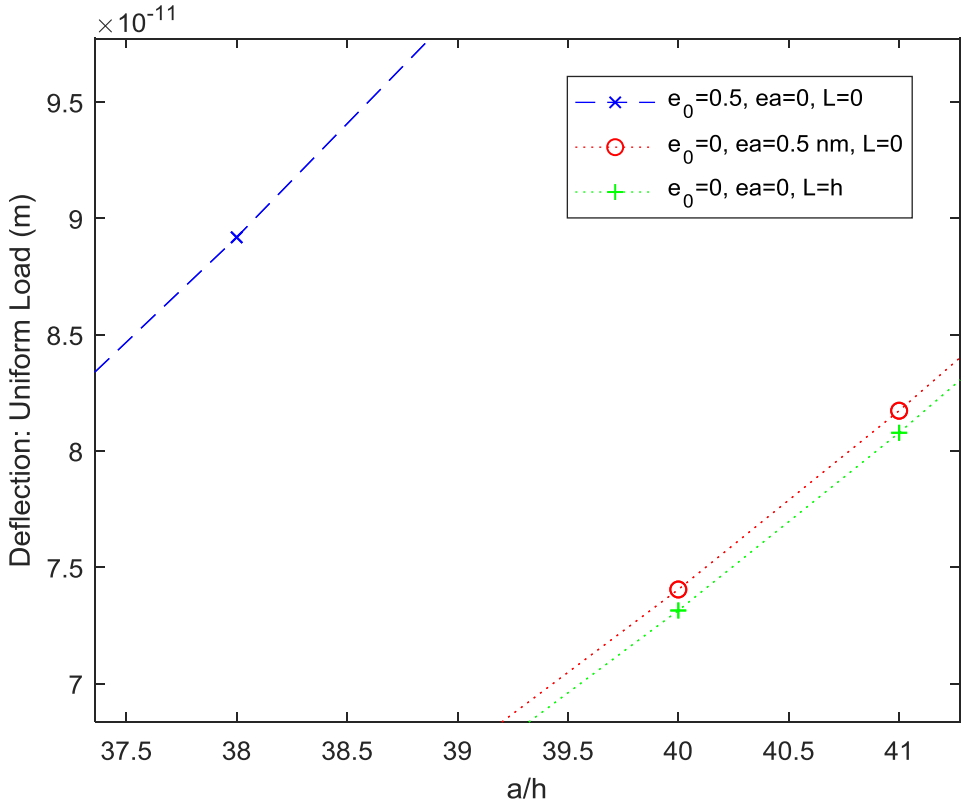

(b)

Fig. 6 Effectiveness rate of porosity coefficient, Eringen's nonlocal parameter and length scale parameter on the deflection caused by uniform loading of a simply supported FG-SWCNTs-reinforced plate with $h = 20$ nm: (a) for $10 < \frac{a}{h} < 50$ (b) for $37.5 < \frac{a}{h} < 41$

Table 8 Critical buckling load N_{cr}(N (newton)) of a simply supported FG-SWCNTs-reinforced plate with various values of porosity coefficient (e_0)

Biaxial buckling ($\gamma_1=\gamma_2=-1$) a/h	r/h	$e_0=0.2$	$e_0=0.5$	$e_0=0.9$
20	0	21.4850	126.1221	265.6382
	0.2	21.5275	126.3711	266.1626
	0.5	21.7501	127.6781	268.9154
	0.8	22.1636	130.1054	274.0278
	1	22.5453	132.3460	278.7470
30	0	23.8042	91.6926	182.2104
	0.2	23.8251	91.7730	182.3702
	0.5	23.9347	92.1953	183.2094
	0.8	24.1384	92.9796	184.7680
	1	24.3263	93.7036	186.2067
40	0	21.4085	71.6236	138.5771
	0.2	21.41990	71.6589	138.6455
	0.5	21.4745	71.8445	139.0045
	0.8	21.5775	72.1891	139.6712
	1	21.6726	72.5072	140.2867
Uniaxial buckling ($\gamma_1=-1,\gamma_2=0$) a/h	r/h	$e_0=0.2$	$e_0=0.5$	$e_0=0.9$
20	0	42.9701	252.2443	531.2765
	0.2	43.0549	252.7422	532.3252
	0.5	43.5002	255.3562	537.8308
	0.8	44.3272	260.2108	548.2108
	1	45.0906	264.6920	557.4939
30	0	47.6084	183.3851	364.4207
	0.2	47.6502	183.5460	364.7404
	0.5	47.8695	184.3907	366.4189
	0.8	48.2767	185.9593	369.5360
	1	48.6526	187.4072	372.4134
40	0	42.8170	143.2472	277.1542
	0.2	42.8381	143.3179	277.2910
	0.5	42.9490	143.6890	278.0090
	0.8	43.1550	144.3782	279.3425
	1	43.3452	145.0145	280.5734

Table 9 Critical buckling load N_{cr} (N (newton)) of a simply supported FG-SWCNTs-reinforced plate with various values Eringen's nonlocal parameter with $h=20$ nm and $e_0=0.5$

Biaxial buckling ($\gamma_1=\gamma_2=-1$) a/h	r/h	$ea=0$	$ea=0.5\ nm$	$ea=1\ nm$	$ea=1.5\ nm$	$ea=2\ nm$
10	0	10.8084	10.8071	10.8031	10.7964	10.7871
	0.5	11.3418	11.3405	11.3362	11.3292	11.3195
	1	12.9420	12.9404	12.9355	12.9276	12.9164
20	0	5.4189	7.4187	7.4180	7.4169	7.4153
	0.5	7.5105	7.5102	7.5095	7.5084	7.5068
	1	7.7851	7.7848	7.7841	7.7829	7.7812
30	0	5.3937	5.3936	5.3933	5.3930	5.3925
	0.5	5.4232	5.4232	5.4230	5.4226	5.4221
	1	5.5120	5.5120	5.5117	5.5113	5.5108
40	0	4.2131	4.2131	4.2130	4.2129	4.2126
	0.5	4.2261	4.2261	4.2260	4.2258	4.2256
	1	4.2651	4.2651	4.2650	4.2648	4.2646
Uniaxial buckling ($\gamma_1=-1,\ \gamma_2=0$) a/h	r/h	$ea=0$	$ea=0.5\ nm$	$ea=1\ nm$	$ea=1.5\ nm$	$ea=2\ nm$
10	0	21.6169	21.6143	21.6063	21.5929	21.5743
	0.5	22.6837	22.6809	22.6725	22.6585	22.6389
	1	25.8839	25.8808	25.8711	25.8552	25.8329
20	0	14.8379	14.8374	14.8360	14.8338	14.8306
	0.5	15.0209	15.0205	15.0191	15.0168	15.0135
	1	15.5701	15.5696	15.5682	15.5658	15.5642
30	0	10.7873	10.7872	10.7868	10.7860	10.7850
	0.5	10.8465	10.8464	10.8459	10.8452	10.8441
	1	11.0239	11.0238	11.0233	11.0226	11.0215
40	0	8.4263	8.4262	8.420	8.4257	8.4253
	0.5	8.4523	8.4522	8.4520	8.4517	8.4512
	1	8.5303	8.5302	8.5300	8.5299	8.5292

In Table 9, the critical buckling load caused by biaxial and uniaxial buckling are presented with various values of Eringen's nonlocal parameter, material length scale parameter and aspect ratio. It is observed from Table 9 that critical buckling load decreases with an increase in Eringen's nonlocal parameter and aspect ratio, and also it increases by increasing of material length scale parameter.

It is observed from Figures 7 to 9 that critical buckling load caused by uniaxial buckling is more than the other case with biaxial buckling. Figure 9 (a) indicates the effect of Eringen's nonlocal parameter on the critical buckling load (uniaxial and biaxial buckling) of a simply supported square plate reinforced by FG-SWCNTs with $h=20$ nm, and $e_0=0.5$. It can be seen that the deflection of CPT decreases by increasing of the Eringen's nonlocal parameter (see Figure 9 (b)).

The effect of porosity coefficient on the increase of the critical buckling load is greatly higher than the other parameters effect, and the material length scale parameter and the Eringen's nonlocal parameter have a lower effect on the critical buckling load increase than the porosity coefficient, respectively (See Figure 10).

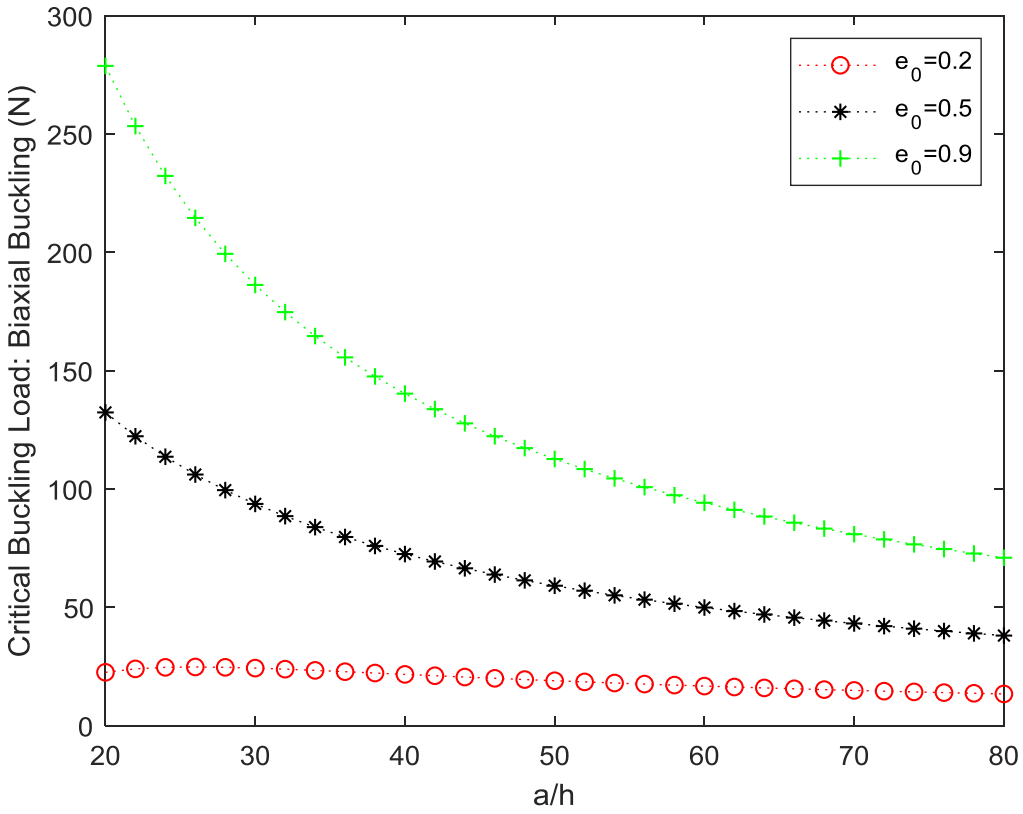

(a)

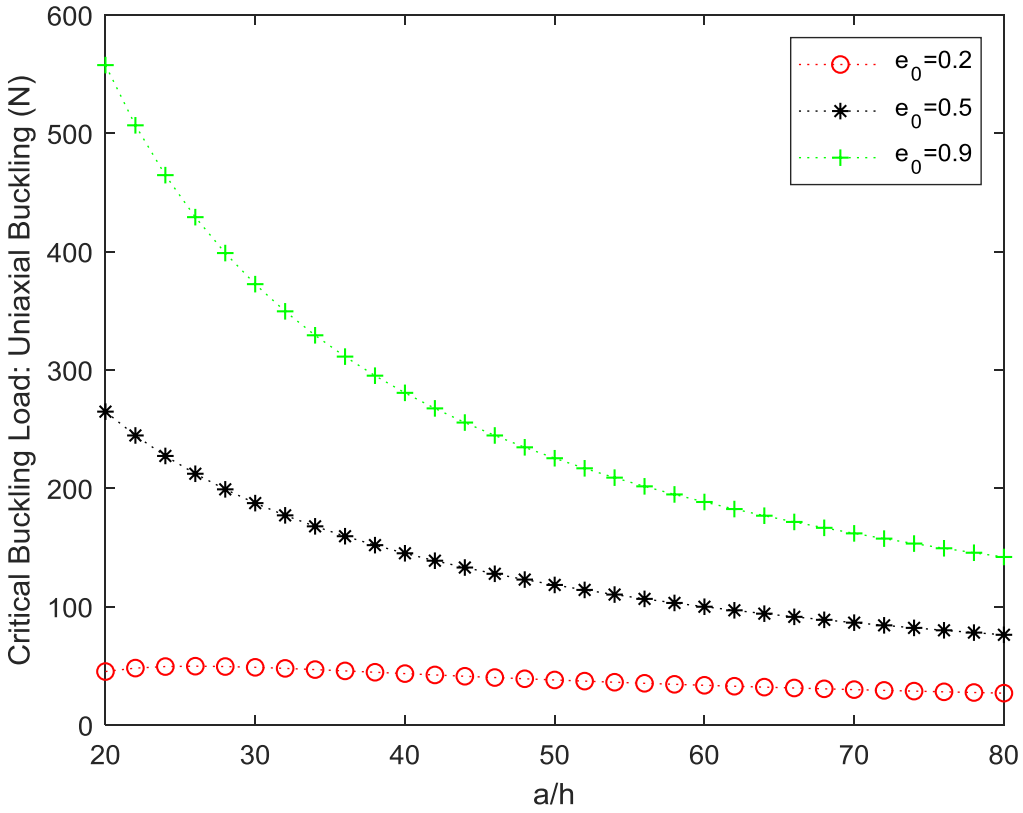

(b)

Fig. 7 Effect of porosity coefficient on the critical buckling load of a simply supported FG-SWCNTs-reinforced plate: (a) biaxial buckling (b) uniaxial buckling

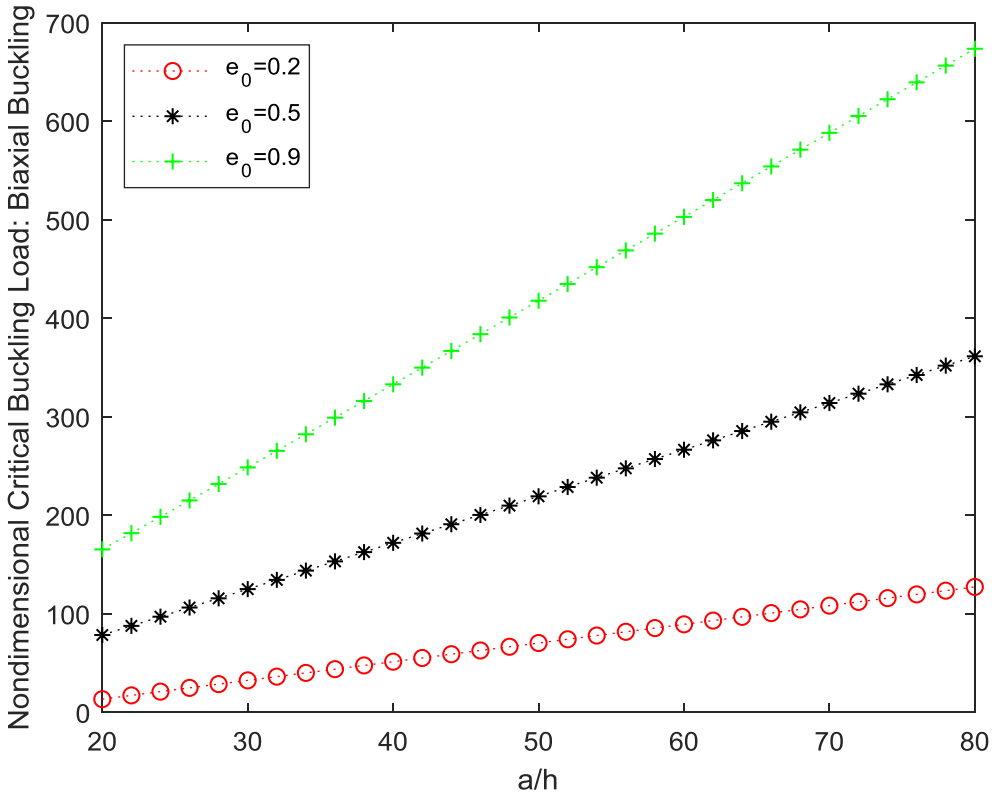

(a)

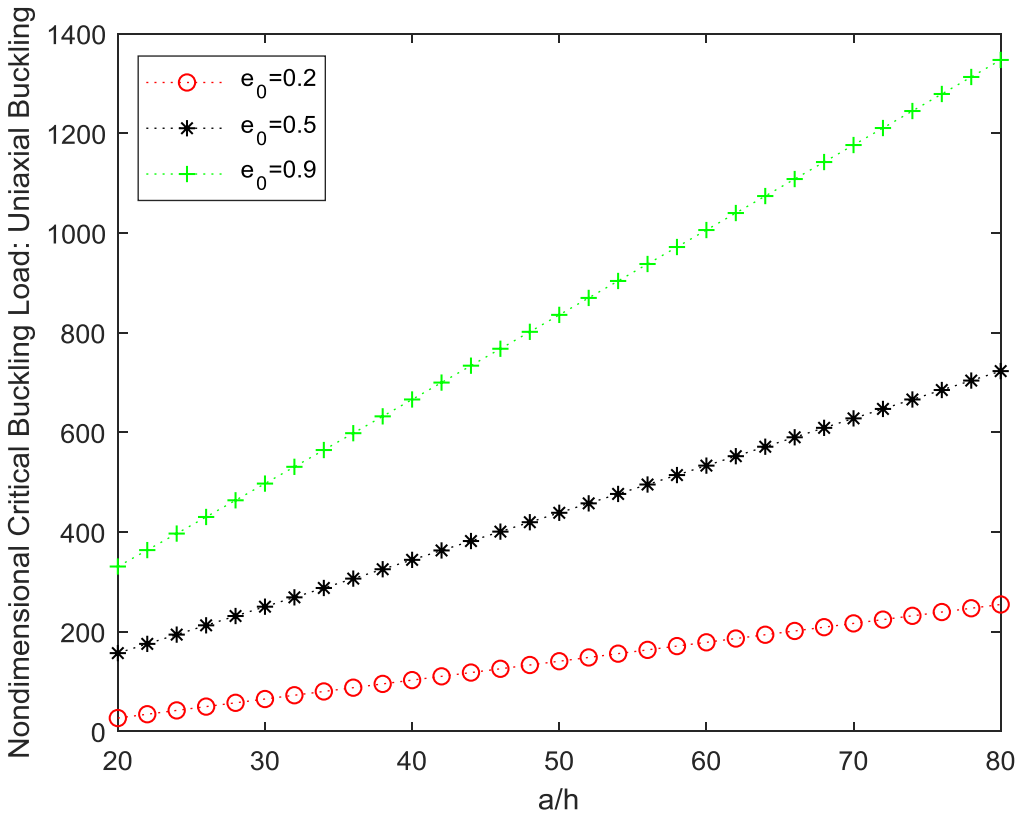

(b)

Fig. 8 Effect of porosity coefficient on the nondimensional critical buckling load of a simply supported FG-SWCNTs-reinforced plate: (a) biaxial buckling (b) uniaxial buckling

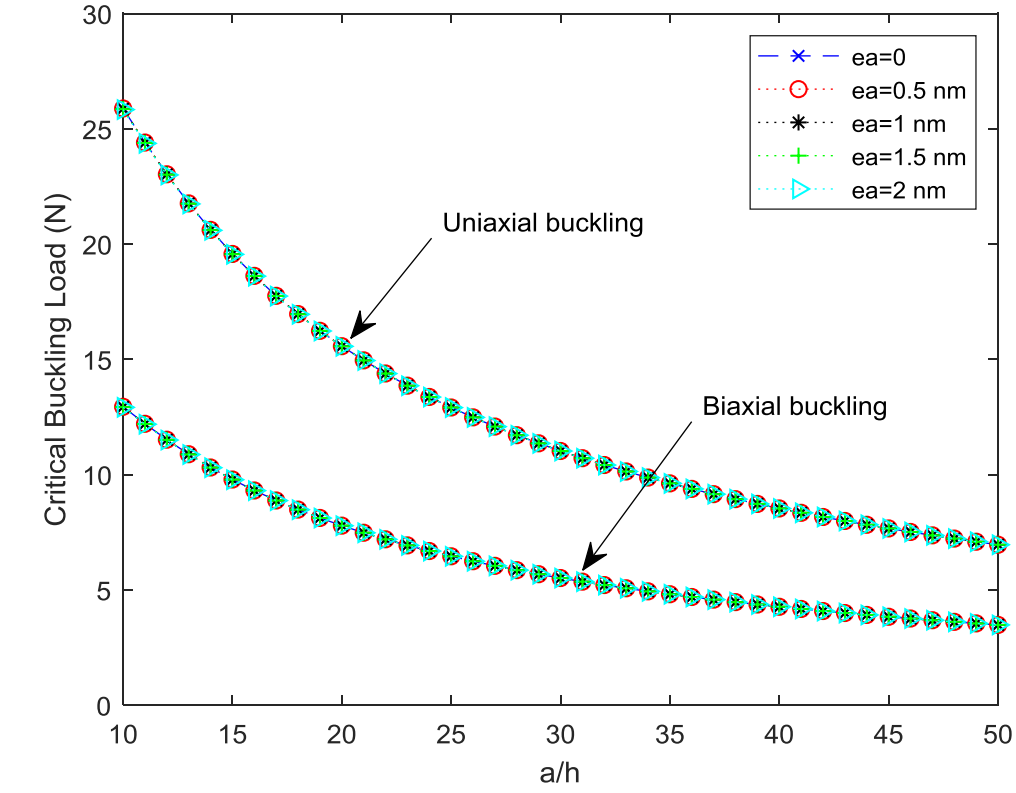

(a)

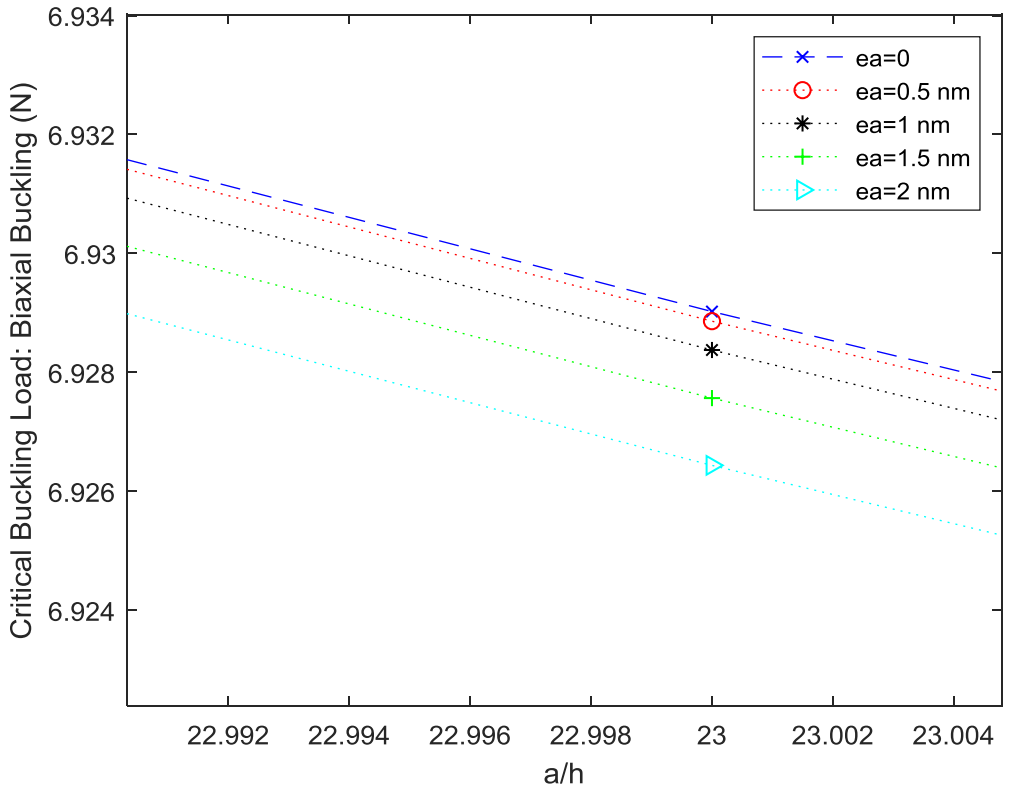

(b)

Fig. 9 Effect of Eringen's nonlocal parameter on the critical buckling load of a simply supported FG-SWCNTs-reinforced plate with $h = 20$ nm, and $e_0 = 0.5$: (a) biaxial and uniaxial buckling (b) biaxial buckling

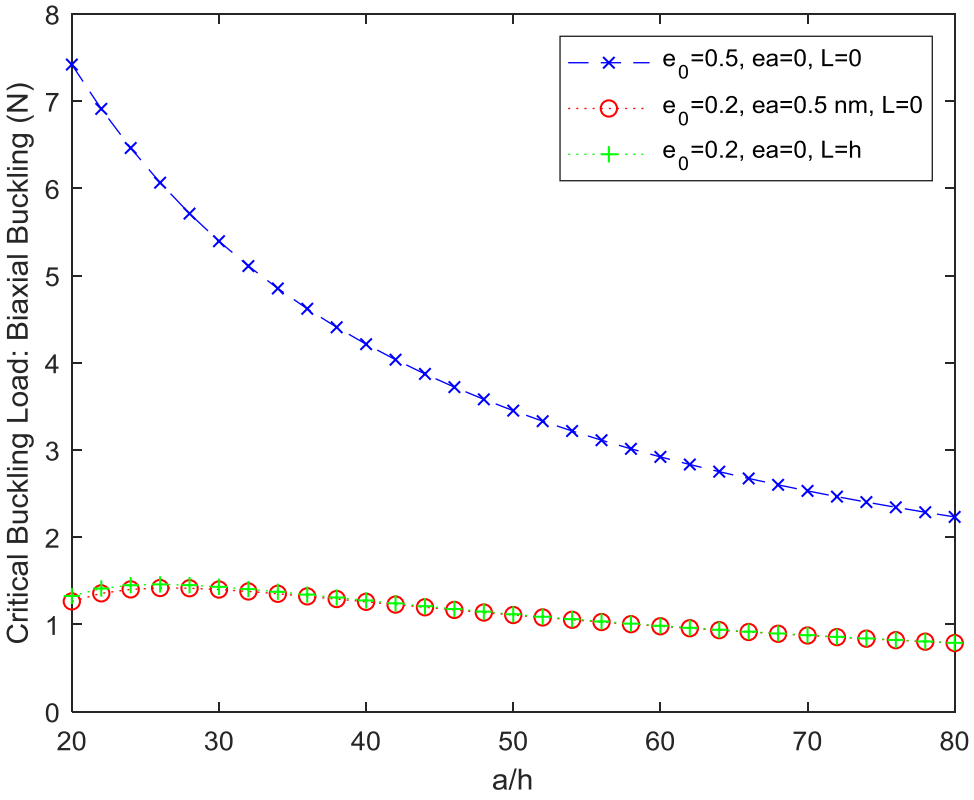

(a)

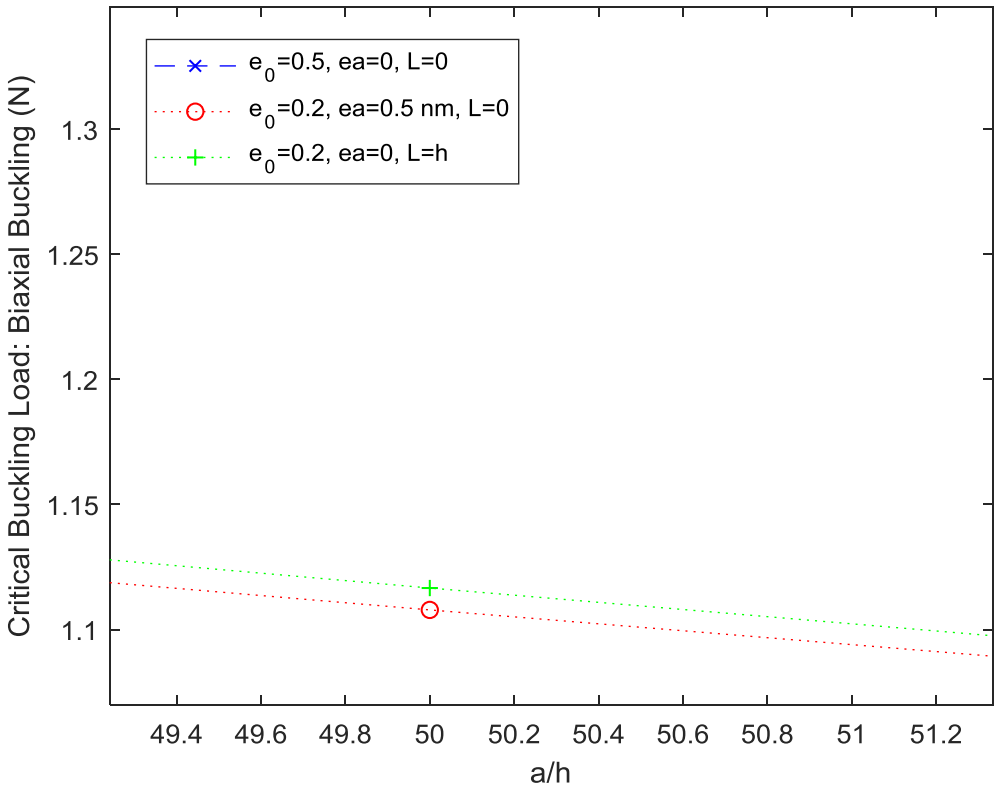

(b)

Fig. 10 Effectiveness rate of porosity coefficient, Eringen's nonlocal parameter and length scale parameter on the critical buckling load caused by biaxial buckling of a simply supported FG-SWCNTs-reinforced plate with $h = 20$ nm: (a) for $20 < \frac{a}{h} < 50$ (b) for $49.4 < \frac{a}{h} < 51.2$

7. Conclusion

This study presents the effects and also the effectiveness rate of material length scale parameter, Eringen's nonlocal parameter, porosity coefficient and aspect ratio on the deflection and critical buckling load of a porous nanocomposite piezoelectric plate reinforced by carbon nanotubes. In order for these investigations, the size dependent effect is employed to consider the nonlocal strain gradient theory for porous nanocomposite piezoelectric plate. The results showed that the critical buckling load decreases with an increase in the Eringen's nonlocal parameter and aspect ratio and vice versa for deflection. Also, the critical buckling load increases with an increase in the material length scale parameter and vice versa for deflection. Furthermore, by increasing of porosity coefficient, stiffness of the plate decreases and as a result deflection increases. The numerical results indicate that the effect of porosity coefficient on the changes of the deflection and critical buckling load is greatly higher than the other parameters effect, and the Eringen's nonlocal parameter and the material length scale parameter have a lower effect on the deflection and vice versa for critical buckling load. It is shown that the critical buckling load caused by uniaxial buckling is more than the other case with biaxial buckling. Also, for deflection, it can be said that the deflection caused by uniform loading is more than the other case with sinusoidal loading.

Acknowledgment

The authors would like to thank the referees for their valuable comments. Also, they are thankful to the the Iranian Nanotechnology Development Committee for their financial support and the University of Kashan for supporting this work by Grant No. 682561/28.

References

Aghababaei, R. and Reddy, JN. (2009), "Nonlocal third-order shear deformation plate theory with application to bending and vibration of plates", *J. Sound Vib.,* **326**(1-2), 277-289, https://doi.org/10.1016/j.jsv.2009.04.044.

AkhavanAlavi S. M., Mohammadimehr M., Edjtahed SH. (2019) "Active control of micro Reddy beam integrated with functionally graded nanocomposite sensor and actuator based on linear quadratic regulator method", *Euro. J. Mech. A/Solids,* **74**, 449-461. https://doi.org/10.1016/j.euromechsol.2018.12.008.

Alavi, SH. and Eipakchi, H. (2019), "Geometry and load effects on transient response of a VFGM annular plate: An analytical approach", *Struct. Eng. Mech.,* **70**(2), 179-197, https://doi.org/10.12989/sem.2019.70.2.179.

Alizada, A.N. and Sofiyev, A.H. (2011), "Modified Young's moduli of nano-materials taking into account the scale effects and vacancies", *Meccanica,* **46**(5), 915-920, https://doi.org/10.1007/s11012-010-9349-1.

Apuzzo, A., Barretta R., Faghidian, SA., Luciano, R. and De Sciarra, FM. (2018), "Free vibrations of elastic beams by modified nonlocal strain gradient theory", *Int. J. Eng. Sci.,* **133**, 99-108. https://doi.org/10.1016/j.ijengsci.2018.09.002.

Arani, AG. and Jalaei, MH. (2017), "Investigation of the longitudinal magnetic field effect on dynamic response of viscoelastic graphene sheet based on sinusoidal shear deformation theory", *Physica B Cond Matter,* **506**, 94-104, https://doi.org/10.1016/j.physb.2016.11.004.

Arani, AG., Jamali, M., Mosayyebi, M. and Kolahchi, R. (2016), "Wave propagation in FG-CNT-reinforced piezoelectric composite micro plates using viscoelastic quasi-3D sinusoidal shear deformation theory", *Compos. Part B Eng.,* **95**, 209-224, https://doi.org/10.1016/j.compositesb.2016.03.077.

Arani, AG., Kolahchi, R. and Vossough, H. (2012), "Buckling analysis and smart control of SLGS using elastically coupled PVDF nanoplate based on the nonlocal Mindlin plate theory", *Physica B Cond. Matter,* **407**(22), 4458-4465, https://doi.org/10.1016/j.physb.2012.07.046.

Arefi, M., Kiani, M. and Rabczuk, T. (2019), "Application of nonlocal strain gradient theory to size dependent bending analysis of a sandwich porous nanoplate integrated with piezomagnetic face-sheets", *Compos. Part B Eng.,* **168**, 320-333, https://doi.org/10.1016/j.compositesb.2019.02.057.

Barretta, R., and Sciarra, F.M.D. (2018), "Constitutive boundary conditions for nonlocal strain gradient elastic nano-beams", *Int. J. Eng. Sci.,* **130**, 187-198. https://doi.org/10.1016/j.ijengsci.2018.05.009.

Barretta, R., Faghidian, S.A. and Sciarra, F.M. D. **(**2019**),** "Stress-driven nonlocal integral elasticity for axisymmetric nano-plates", *Int. J. Eng. Sci.,* **136**, 38-52, https://doi.org/10.1016/j.ijengsci.2019.01.003.

Batra, RC. (2007), "Higher-order shear and normal deformable theory for functionally graded incompressible linear elastic plates", *Thin-Walled Struct.,* **45**(12), 974-982, https://doi.org/10.1016/j.tws.2007.07.008.

Batra, RC. and Aimmanee, S. (2005), "Vibrations of thick isotropic plates with higher order shear and normal deformable plate theories", *Comput. Struct.,* **83**(12-13), 934-955, https://doi.org/10.1016/j.compstruc.2004.11.023.

Batra, RC. and Aimmanee, S. (2007), "Vibration of an incompressible isotropic linear elastic rectangular plate with a higher-order shear and normal deformable theory", *J. Sound Vib.,* **307**(3-5), 961-971, https://doi.org/110.1016/j.jsv.2007.06.064.

Batra, RC., Vidoli, S. and Vestroni, F. (2002), "Plane wave solutions and modal analysis in higher order shear and normal deformable plate theories", *J. Sound Vib.,* **257**(1), 63-88, https://doi.org/10.1006/jsvi.2002.5029.

Ebrahimi, F. and Barati, MR. (2018), "Damping vibration analysis of graphene sheets on viscoelastic medium incorporating hygro-thermal effects employing nonlocal strain gradient theory", *Compos. Struct.,* **185**, 241-253, https://doi.org/10.1016/j.compstruct.2017.10.021.

Ebrahimi, F., Seyfi, A. and Tornabene, F. (2019), "Wave dispersion characteristics of porous graphene platelet-reinforced composite shells", *Struct. Eng. Mech.,* **71**(1), 99-107, https://doi.org/10.12989/sem.2019.71.1.099.

Gholami, R. and Ansari, R. (2017), "A unified nonlocal nonlinear higher-order shear deformable plate model for postbuckling analysis of piezoelectric-piezomagnetic rectangular nanoplates with various edge supports", *Compos. Struct.,* **166**, 202-218, https://doi.org/10.1016/j.compstruct.2017.01.045.

Ghorbanpour Arani A., Rousta Navi B., Mohammadimehr M. (2016) "Surface stress and agglomeration effects on nonlocal biaxial buckling polymeric nanocomposite plate reinforced by CNT using various approaches", *Adv. Compos. Mater.,* **25**(5), 423-441. https://doi.org/10.1080/09243046.2015.1052189

Jomehzadeh, E., Noori, HR. and Saidi, AR. (2011), "The size-dependent vibration analysis of micro-plates based on a modified couple stress theory", *Physica E: Low-dimens. Sys. Nanostruct.,* **43**(4), 877-883, https://doi.org/10.1016/j.physe.2010.11.005.

Kim, J., Żur, KK. and Reddy, JN. (2019), "Bending, free vibration, and buckling of modified couples stress-based functionally graded porous micro-plates", *Compos. Struct.,* **209**, 879-888, https://doi.org/10.1016/j.compstruct.2018.11.023.

Li, L., Hu, Y. and Ling, L. (2016), "Wave propagation in viscoelastic single-walled carbon nanotubes with surface effect under magnetic field based on nonlocal strain gradient theory", *Physica E: Low-dimens. Sys. Nanostruct.,* **75**, 118-124, https://doi.org/10.1016/j.physe.2015.09.028.

Lu, L., Guo, X. and Zhao, J. (2017), "Size-dependent vibration analysis of nanobeams based on the nonlocal strain gradient theory", *Int. J. Eng. Sci.,* **116**, 12-24, https://doi.org/10.1016/j.ijengsci.2017.03.006.

Lu, L., Guo, X. and Zhao, J. (2019), "A unified size-dependent plate model based on nonlocal strain gradient theory including surface effects", *Appl. Math. Model.,* **68**, 583-602, https://doi.org/10.1016/j.apm.2018.11.023.

Mahinzare, M., Alipour, MJ., Sadatsakkak, SA. and Ghadiri, M. (2019), "A nonlocal strain gradient theory for dynamic modeling of a rotary thermo piezo electrically actuated nano FG circular plate", *Mech. Sys. Signal Proces.,* **115**, 323-337, https://doi.org/10.1016/j.ymssp.2018.05.043.

Magnucka-Blandzi, E. (2008), "Axi-symmetrical deflection and buckling of circular porous-cellular plate", *Thin-Walled Struct*., **46**(3), 333-337, https://doi.org/10.1016/j.tws.2007.06.006.

Malikan, M., Nguyen, VB. and Tornabene, F. (2018), "Damped forced vibration analysis of single-walled carbon nanotubes resting on viscoelastic foundation in thermal environment using nonlocal strain gradient theory", *Eng. Sci. Technol.,* **21**(4), 778-786, https://doi.org/10.1016/j.jestch.2018.06.001.

Mao, JJ. and Zhang, W. (2019), "Buckling and post-buckling Analyses of Functionally Graded Graphene Reinforced Piezoelectric Plate Subjected to Electric Potential and Axial Forces", *Compos. Struct.,* **216**, 392-405, https://doi.org/10.1016/j.jestch.2018.06.001.

Mohammadimehr, M., Navi, BR. and Arani AG. (2015), "Free vibration of viscoelastic double-bonded polymeric nanocomposite plates reinforced by FG-SWCNTs using MSGT, sinusoidal shear deformation theory and meshless method", *Compos. Struct.,* **131**, 654-671, https://doi.org/10.1016/j.compstruct.2015.05.077.

Mohammadimehr, M., Mohammadi Najafabadi, MM., Nasiri, H. and Rousta Navi, B. (2016a), "Surface stress effects on the free vibration and bending analysis of the nonlocal single-layer graphene sheet embedded in an elastic medium using energy method", *Proc. Ins. Mech. Eng. Part N: J. Nanomater, Nanoeng and Nanosys,* **230**(3), 148-160, https://doi.org/10.1177/1740349914559042.

Mohammadimehr, M., Navi, BR. and Arani, AG. (2016b), "Modified strain gradient Reddy rectangular plate model for biaxial buckling and bending analysis of double-coupled piezoelectric polymeric nanocomposite reinforced by FG-SWNT", *Compos. Part B Eng.,* **87**, 132-148, https://doi.org/10.1016/j.compositesb.2015.10.007.

Mohammadimehr, M., Salemi, M. and Navi, BR. (2016c), "Bending, buckling, and free vibration analysis of MSGT microcomposite Reddy plate reinforced by FG-SWCNTs with temperature-dependent material properties under hydro-thermo-mechanical loadings using DQM", *Compos. Struct.,* **138**, 361-380, https://doi.org/10.1016/j.compstruct.2015.11.055.

Mohammadimehr, M., Nejad, ES. and Mehrabi M. (2018), "Buckling and vibration analyses of MGSGT double-bonded micro composite sandwich SSDT plates reinforced by CNTs and BNNTs with isotropic foam & flexible transversely orthotropic cores", *Struct. Eng. Mech.,* **65**(4), 491-504, https://doi.org/10.12989/sem.2018.65.4.491.

Mohammadimehr M., Shahedi S., Rousta Navi B. (2017a) "Nonlinear vibration analysis of FG-CNTRC sandwich Timoshenko beam based on modified couple stress theory subjected to longitudinal magnetic field using generalized differential quadrature method", *Proc Inst Mech Eng, Part C: J. Mech. Eng. Sci.,* **231**(20), 3866-3885. https://doi.org/10.1177/0954406216653622

Mohammadimehr M., Navi BR., Ghorbanpour Arani A. (2017b) "Dynamic stability of modified strain gradient theory sinusoidal viscoelastic piezoelectric polymeric functionally graded single-walled carbon nanotubes reinforced nanocomposite plate considering surface stress and agglomeration effects under hydro-thermo-electro-magneto-mechanical loadings", *Mech. Adv. Mater. Struct.,* **24**(16), 1325-1342. https://doi.org/10.1080/15376494.2016.1227507

Mohammadimehr M., Alimirzaei S. (2016) "Nonlinear static and vibration analysis of Euler-Bernoulli composite beam model reinforced by FG-SWCNT with initial geometrical imperfection using FEM", *Struct. Eng. Mech.,* **59**(3), 431-454. https://doi.org/10.12989/sem.2016.59.3.431

Mohammadimehr M., Mohammadimehr MA., Dashti P. (2016d) "Size-dependent effect on biaxial and shear nonlinear buckling analysis of nonlocal isotropic and orthotropic micro-plate based on surface stress and modified couple stress theories using differential quadrature method", *Appl. Math. Mech.,* **37**(4), 529-554. https://doi.org/10.1007/s10483-016-2045-9

Mohammadzadeh, B., Choi, E. and Kim, D. (2019), "Vibration of sandwich plates considering elastic foundation, temperature change and FGM faces", *Struct. Eng. Mech.,* **70**(5), 591-600, https://doi.org/10.12989/sem.2019.70.5.591.

Reddy, JN. (2010), "Nonlocal nonlinear formulations for bending of classical and shear deformation theories of beams and plates", *Int. J. Eng. Sci.,* **48**(11), 1507-1518, https://doi.org/10.1016/j.ijengsci.2010.09.020.

Reddy, J.N. (2017), "Energy principles and variational methods in applied mechanics", *J. W. S.*

Reddy, JN. and Kim J. (2012), "A nonlinear modified couple stress-based third-order theory of functionally graded plates", *Compos. Struct.,* **94**(3), 1128-1143, https://doi.org/10.1016/j.compstruct.2011.10.006.

Rezaei, AS. and Saidi, AR. (2015), "Exact solution for free vibration of thick rectangular plates made of porous materials", *Compos. Struct.,* **134**, 1051-1060, https://doi.org/10.1016/j.compstruct.2015.08.125.

Rezaei, AS., Saidi, AR., Abrishamdari, M. and Mohammadi MP. (2017), "Natural frequencies of functionally graded plates with porosities via a simple four variable plate theory: an analytical approach", *Thin-Walled Struct.,* **120**, 366-377, https://doi.org/10.1016/j.tws.2017.08.003.

Rajabi, J., Mohammadimehr, M. (2019) "Bending analysis of a micro sandwich skew plate using extended Kantorovich method based on Eshelby-Mori-Tanaka approach", *Comput.Concrete,* **23**(5), pp. 361-376, https://doi.org/10.12989/cac.2019.23.5.361

Saidi, AR., Rasouli, A. and Sahraee, S. (2009), "Axisymmetric bending and buckling analysis of thick functionally graded circular plates using unconstrained third-order shear deformation plate theory", *Compos. Struct.,* **89**(1), 110-119, https://doi.org/10.1016/j.compstruct.2008.07.003.

She, GL., Yuan, FG., Ren, YR., Liu, HB. and Xiao, WS. (2018), "Nonlinear bending and vibration analysis of functionally graded porous tubes via a nonlocal strain gradient theory", *Compos. Struct.,* **203**, 614-623, https://doi.org/10.1016/j.compstruct.2018.07.063.

Shen, H.S. (2009), "Nonlinear bending of functionally graded carbon nanotube-reinforced composite plates in thermal environments", *Compos. Struct.,* **91**(1), 9-19, https://doi.org/10.1016/j.compstruct.2009.04.026.

Shen, H.S., and Zhang, C.L. (2010), "Thermal buckling and postbuckling behavior of functionally graded carbon nanotube-reinforced composite plates", *Mater. Design,* **31**, 3403–3411, https://doi.org/10.1016/j.matdes.2010.01.048

Sofiyev, A.H., Turkaslan, B.E., Bayramov, R.P. and Salamci, M.U. (2019), "Analytical solution of stability of FG-CNTRC conical shells under external pressures", *Thin-Walled Struct.,* **144**, 106338, https://doi.org/10.1016/j.tws.2019.106338.

Tanzadeh, H. and Amoushahi, H. (2019), "Buckling and free vibration analysis of piezoelectric laminated composite plates using various plate deformation theories", *Europ. J. Mech.-A/Solids,* **74**, 242-256, https://doi.org/10.1016/j.euromechsol.2018.11.013.

Thai, HT. and Choi, DH. (2013), "Size-dependent functionally graded Kirchhoff and Mindlin plate models based on a modified couple stress theory", *Compos. Struct.,* **95**, 142-153, https://doi.org/10.1016/j.compstruct.2012.08.023.

Thai, H.T. and Kim, S.E. (2013), "A size-dependent functionally graded Reddy plate model based on a modified couple stress theory", *Compos. Part B: Eng.,* **45**(1), 1636-1645, https://doi.org/10.1016/j.compositesb.2012.09.065.

Van, D.T., Nguyen, D.K., Duc, N.D., Doan, D.H. and Bui, T.Q. (2017), "Analysis of bi-directional functionally graded plates by FEM and a new third-order shear deformation plate theory", *Thin-Walled Struct.,* **119**, 687-699.

Wang, Q. (2002), "On buckling of column structures with a pair of piezoelectric layers", *Eng. Struct.,* **24**(2), 199-205, https://doi.org/10.1016/S0141-0296(01)00088-8.

Wang, B., Zhou, S., Zhao, J. and Chen, X. (2011), "A size-dependent Kirchhoff micro-plate model based on strain gradient elasticity theory", *Europ. J. Mech.-A/Solids,* **30**(4) 517-524, https://doi.org/10.1016/j.tws.2017.07.022.

Yang, J., Chen, D. and Kitipornchai, S. (2018), "Buckling and free vibration analyses of functionally graded graphene reinforced porous nanocomposite plates based on Chebyshev-Ritz method", *Compos. Struct.,* **193**, 281-294, https://doi.org/10.1016/j.compstruct.2018.03.090.

Yazdani, R., Mohammadimehr, M. and Rousta Navi, B. (2019), "Free vibration of Cooper-Naghdi micro saturated porous sandwich cylindrical shells with reinforced CNT face sheets under magneto-hydro-thermo-mechanical loadings", *Struct. Eng. Mech.,* **70**(3), 351-365, https://doi.org/10.12989/sem.2019.70.3.351.

Yin, L., Qian, Q., Wang, L. and Xia, W. (2010), "Vibration analysis of microscale plates based on modified couple stress theory", *Acta Mech. Solida Sinica*, **23**(5), 386-393, https://doi.org/10.1016/S0894-9166(10)60040-7.

Zenkour, AM. and Alghanmi, RA. (2019), "Stress analysis of a functionally graded plate integrated with piezoelectric faces via a four-unknown shear deformation theory", *Results Phys.,* **12**, 268-277, https://doi.org/10.1016/j.rinp.2018.11.045.

Zenkour, AM. and Radwan, AF. (2018), "Compressive study of functionally graded plates resting on Winkler–Pasternak foundations under various boundary conditions using hyperbolic shear deformation theory", *Arch. Civil Mech. Eng.,* **18**(2), 645-658, https://doi.org/10.1016/j.acme.2017.10.003.

Zhu, P., Lei, Z.X. and Liew, K.M. (2012), "Static and free vibration analyses of carbon nanotube-reinforced composite plates using finite element method with first order shear deformation plate theory", *Compos. Struct*., **94**(4), 1450-1460, https://doi.org/10.1016/j.compstruct.2011.11.010.

Appendix A

$$
\begin{aligned}
&A_x^{(i)} = \int E_{x_{(z)}} z^{(i)} dz \qquad B^{(i)} = \int z^{(i)} dz \\
&A_y^{(i)} = \int E_{y_{(z)}} z^{(i)} dz \qquad C^{(i)} = \int z^{(i)} \sin(\beta' z) dz \\
&A_{xy}^{(i)} = \int E_{xy_{(z)}} z^{(i)} dz \qquad D^{(i)} = \int z^{(i)} \cos(\beta' z) dz \\
&i = 0,1,2
\end{aligned}
\tag{A-1}
$$

Appendix B

$$
\begin{aligned}
N_x = {} & \frac{1}{1-\upsilon^2} \times \\
& \left(A_x^0 \frac{\partial u_0}{\partial x} - A_x^1 \frac{\partial^2 w}{\partial x^2} + A_x^0 \frac{1}{2} (\frac{\partial w}{\partial x})^2 + \upsilon \left(A_x^0 \frac{\partial v_0}{\partial y} - A_x^1 \frac{\partial^2 w}{\partial y^2} + A_x^0 \frac{1}{2} (\frac{\partial w}{\partial y})^2 \right) \right. \\
& - \ell^2 \left(\begin{array}{l} A_x^0 \frac{\partial^3 u_0}{\partial x^3} - A_x^1 \frac{\partial^4 w}{\partial x^4} + A_x^0 \frac{1}{2} \frac{\partial^2 (\partial w / \partial x)^2}{\partial x^2} + \upsilon \left(\begin{array}{l} A_x^0 \frac{\partial^3 v_0}{\partial x^2 \partial y} - A_x^1 \frac{\partial^4 w}{\partial x^2 \partial y^2} \\ + A_x^0 \frac{1}{2} \frac{\partial^2 (\partial w / \partial y)^2}{\partial x^2} \end{array} \right) \\ + A_x^0 \frac{\partial^3 u_0}{\partial x \partial y^2} - A_x^1 \frac{\partial^4 w}{\partial x^2 \partial y^2} + A_x^0 \frac{1}{2} \frac{\partial^2 (\partial w / \partial x)^2}{\partial y^2} + \upsilon \left(\begin{array}{l} A_x^0 \frac{\partial^3 v_0}{\partial y^3} - A_x^1 \frac{\partial^4 w}{\partial y^4} \\ + A_x^0 \frac{1}{2} \frac{\partial^2 (\partial w / \partial y)^2}{\partial y^2} \end{array} \right) \end{array} \right) \\
& \left. + \frac{(ea)^2}{1-\upsilon^2} \times \right. \\
& \left(A_x^0 \frac{\partial^3 u_0}{\partial x^3} - A_x^1 \frac{\partial^4 w}{\partial x^4} + A_x^0 \frac{1}{2} \frac{\partial^2 (\partial w / \partial x)^2}{\partial x^2} + \upsilon \left(\begin{array}{l} A_x^0 \frac{\partial^3 v_0}{\partial x^2 \partial y} - A_x^1 \frac{\partial^4 w}{\partial x^2 \partial y^2} \\ + A_x^0 \frac{1}{2} \frac{\partial^2 (\partial w / \partial y)^2}{\partial x^2} \end{array} \right) \right. \\
& - \ell^2 \left(\begin{array}{l} A_x^0 \frac{\partial^5 u_0}{\partial x^5} - A_x^1 \frac{\partial^6 w}{\partial x^6} + A_x^0 \frac{1}{2} \frac{\partial^4 (\partial w / \partial x)^2}{\partial x^4} + \upsilon \left(\begin{array}{l} A_x^0 \frac{\partial^5 v_0}{\partial x^4 \partial y} - A_x^1 \frac{\partial^6 w}{\partial x^4 \partial y^2} \\ + A_x^0 \frac{1}{2} \frac{\partial^4 (\partial w / \partial y)^2}{\partial x^4} \end{array} \right) \\ + A_x^0 \frac{\partial^5 u_0}{\partial x^3 \partial y^2} - A_x^1 \frac{\partial^6 w}{\partial x^4 \partial y^2} + A_x^0 \frac{1}{2} \frac{\partial^4 (\partial w / \partial x)^2}{\partial x^2 \partial y^2} \\ + \upsilon \left(A_x^0 \frac{\partial^5 v_0}{\partial x^2 \partial y^3} - A_x^1 \frac{\partial^6 w}{\partial x^2 \partial y^4} + A_x^0 \frac{1}{2} \frac{\partial^4 (\partial w / \partial y)^2}{\partial x^2 \partial y^2} \right) \end{array} \right) \\
& \left. \left. \right) \right)
\end{aligned}
\tag{B-1}
$$

$$
\begin{aligned}
&+\frac{(ea)^2}{1-\upsilon^2}\times\\
&\left(\begin{array}{l}
A_x^0\frac{\partial^3 v_0}{\partial y^3}-A_x^1\frac{\partial^4 w}{\partial y^4}\\
+A_x^0\frac{1}{2}\frac{\partial^2(\partial w/\partial y)^2}{\partial y^2}
\end{array}\right)+\upsilon\left(\begin{array}{l}
A_x^0\frac{\partial^3 u_0}{\partial x\,\partial y^2}-A_x^1\frac{\partial^4 w}{\partial x^2\partial y^2}+A_x^0\frac{1}{2}\frac{\partial^2(\partial w/\partial x)^2}{\partial y^2}\\
-l^2\left(\begin{array}{l}
A_x^0\frac{\partial^5 u_0}{\partial x^3\partial y^2}-A_x^1\frac{\partial^6 w}{\partial x^4\partial y^2}+A_x^0\frac{1}{2}\frac{\partial^4(\partial w/\partial x)^2}{\partial x^2\partial y^2}+\upsilon\left(\begin{array}{l}
A_x^0\frac{\partial^5 v_0}{\partial x^2\partial y^3}-A_x^1\frac{\partial^6 w}{\partial x^2\partial y^4}\\
+A_x^0\frac{1}{2}\frac{\partial^4(\partial w/\partial y)^2}{\partial x^2\partial y^2}
\end{array}\right)\\
+A_x^0\frac{\partial^5 u_0}{\partial x\,\partial y^4}-A_x^1\frac{\partial^6 w}{\partial x^2\partial y^4}+A_x^0\frac{1}{2}\frac{\partial^4(\partial w/\partial x)^2}{\partial y^4}+\upsilon\left(\begin{array}{l}
A_x^0\frac{\partial^5 v_0}{\partial y^5}-A_x^1\frac{\partial^6 w}{\partial y^6}\\
+A_x^0\frac{1}{2}\frac{\partial^4(\partial w/\partial y)^2}{\partial y^4}
\end{array}\right)
\end{array}\right)
\end{array}\right)\\
&-e_{31}\left(-C^0\beta'\phi_E-B^0\frac{2V_E}{h}\right)+\frac{(ea)^2}{1-\upsilon^2}\left(-e_{31}\left(-C^0\beta'\frac{\partial^2\phi_E}{\partial x^2}\right)-e_{31}\left(-C^0\beta'\frac{\partial^2\phi_E}{\partial y^2}\right)\right)
\end{aligned}
\tag{B-1}
$$

$$
\begin{aligned}
&N_y=\frac{1}{1-\upsilon^2}\times\\
&\left(\begin{array}{l}
A_y^0\frac{\partial v_0}{\partial y}-A_y^1\frac{\partial^2 w}{\partial y^2}+A_y^0\frac{1}{2}(\frac{\partial w}{\partial y})^2+\upsilon\left(A_x^0\frac{\partial u_0}{\partial x}-A_x^1\frac{\partial^2 w}{\partial x^2}+A_x^0\frac{1}{2}(\frac{\partial w}{\partial x})^2\right)\\
-l^2\left(\begin{array}{l}
A_y^0\frac{\partial^3 v_0}{\partial x^2\partial y}-A_y^1\frac{\partial^4 w}{\partial x^2\partial y^2}+A_y^0\frac{1}{2}\frac{\partial^2(\partial w/\partial y)^2}{\partial x^2}+\upsilon\left(\begin{array}{l}
A_x^0\frac{\partial^3 u_0}{\partial x^3}-A_x^1\frac{\partial^4 w}{\partial x^4}\\
+A_x^0\frac{1}{2}\frac{\partial^2(\partial w/\partial x)^2}{\partial x^2}
\end{array}\right)\\
+A_y^0\frac{\partial^3 v_0}{\partial y^3}-A_y^1\frac{\partial^4 w}{\partial y^4}+A_y^0\frac{1}{2}\frac{\partial^2(\partial w/\partial y)^2}{\partial y^2}+\upsilon\left(\begin{array}{l}
A_x^0\frac{\partial^3 u_0}{\partial x\,\partial y^2}-A_x^1\frac{\partial^4 w}{\partial x^2\partial y^2}\\
+A_x^0\frac{1}{2}\frac{\partial^2(\partial w/\partial x)^2}{\partial y^2}
\end{array}\right)
\end{array}\right)
\end{array}\right)\\
&+\frac{(ea)^2}{1-\upsilon^2}\times\\
&\left(\begin{array}{l}
A_y^0\frac{\partial^3 v_0}{\partial x^2\partial y}-A_y^1\frac{\partial^4 w}{\partial x^2\partial y^2}+A_y^0\frac{1}{2}\frac{\partial^2(\partial w/\partial y)^2}{\partial x^2}+\upsilon\left(\begin{array}{l}
A_x^0\frac{\partial^3 u_0}{\partial x^3}-A_x^1\frac{\partial^4 w}{\partial x^4}\\
+A_x^0\frac{1}{2}\frac{\partial^2(\partial w/\partial x)^2}{\partial x^2}
\end{array}\right)\\
-l^2\left(\begin{array}{l}
A_y^0\frac{\partial^5 v_0}{\partial x^4\partial y}-A_y^1\frac{\partial^6 w}{\partial x^4\partial y^2}+A_y^0\frac{1}{2}\frac{\partial^4(\partial w/\partial y)^2}{\partial x^4}+\upsilon\left(\begin{array}{l}
A_x^0\frac{\partial^5 u_0}{\partial x^5}-A_x^1\frac{\partial^6 w}{\partial x^6}\\
+A_x^0\frac{1}{2}\frac{\partial^4(\partial w/\partial x)^2}{\partial x^4}
\end{array}\right)\\
+A_y^0\frac{\partial^5 v_0}{\partial x^2\partial y^3}-A_y^1\frac{\partial^6 w}{\partial x^2\partial y^4}+A_y^0\frac{1}{2}\frac{\partial^4(\partial w/\partial y)^2}{\partial x^2\partial y^2}+\upsilon\left(\begin{array}{l}
A_x^0\frac{\partial^5 u_0}{\partial x^3\partial y^2}-A_x^1\frac{\partial^6 w}{\partial x^4\partial y^2}\\
+A_x^0\frac{1}{2}\frac{\partial^4(\partial w/\partial x)^2}{\partial x^2\partial y^2}
\end{array}\right)
\end{array}\right)
\end{array}\right)
\end{aligned}
\tag{B-2}
$$

$$
\begin{aligned}
&+\frac{(ea)^2}{1-\upsilon^2}\times \\
&\left(\begin{array}{l}
A_y^0\frac{\partial^3 v_0}{\partial y^3}-A_y^1\frac{\partial^4 w}{\partial y^4}+A_y^0\frac{1}{2}\frac{\partial^2(\partial w/\partial y)^2}{\partial y^2}+\upsilon\left(\begin{array}{l}A_x^0\frac{\partial^3 u_0}{\partial x\,\partial y^2}-A_x^1\frac{\partial^4 w}{\partial x^2\partial y^2}\\ +A_x^0\frac{1}{2}\frac{\partial^2(\partial w/\partial x)^2}{\partial y^2}\end{array}\right)\\
-\ell^2\left(\begin{array}{l}A_y^0\frac{\partial^5 v_0}{\partial x^2\partial y^3}-A_y^1\frac{\partial^6 w}{\partial x^2\partial y^4}+A_y^0\frac{1}{2}\frac{\partial^4(\partial w/\partial y)^2}{\partial x^2\partial y^2}+\upsilon\left(\begin{array}{l}A_x^0\frac{\partial^5 u_0}{\partial x^3\partial y^2}-A_x^1\frac{\partial^6 w}{\partial x^4\partial y^2}\\ +A_x^0\frac{1}{2}\frac{\partial^4(\partial w/\partial x)^2}{\partial x^2\partial y^2}\end{array}\right)\\
+A_y^0\frac{\partial^5 v_0}{\partial y^5}-A_y^1\frac{\partial^6 w}{\partial y^6}+A_y^0\frac{1}{2}\frac{\partial^4(\partial w/\partial y)^2}{\partial y^4}+\upsilon\left(\begin{array}{l}A_x^0\frac{\partial^5 u_0}{\partial x\,\partial y^4}-A_x^1\frac{\partial^6 w}{\partial x^2\partial y^4}\\ +A_x^0\frac{1}{2}\frac{\partial^4(\partial w/\partial x)^2}{\partial y^4}\end{array}\right)\end{array}\right)
\end{array}\right)\\
&-e_{32}\left(-C^0\beta'\phi_E-B^0\frac{2V_E}{h}\right)+\frac{(ea)^2}{1-\upsilon^2}\left(-e_{32}\left(-C^0\beta'\frac{\partial^2\phi_E}{\partial x^2}\right)-e_{32}\left(-C^0\beta'\frac{\partial^2\phi_E}{\partial y^2}\right)\right)
\end{aligned}
\tag{B-2}
$$

$$
\begin{aligned}
&N_{xy}=\\
&\left(\begin{array}{l}
A_{xy}^0\frac{\partial u_0}{\partial y}+A_{xy}^0\frac{\partial v_0}{\partial x}-2A_{xy}^1\frac{\partial^2 w}{\partial x\,\partial y}+A_{xy}^0\left(\frac{\partial w}{\partial x}\right)\left(\frac{\partial w}{\partial y}\right)\\
-\ell^2\left(\begin{array}{l}A_{xy}^0\frac{\partial^3 u_0}{\partial x^2\partial y}+A_{xy}^0\frac{\partial^3 v_0}{\partial x^3}-2A_{xy}^1\frac{\partial^4 w}{\partial x^3\partial y}+A_{xy}^0\frac{\partial^2\left(\frac{\partial w}{\partial x}\right)\left(\frac{\partial w}{\partial y}\right)}{\partial x^2}\\ +A_{xy}^0\frac{\partial^3 u_0}{\partial y^3}+A_{xy}^0\frac{\partial^3 v_0}{\partial x\,\partial y^2}-2A_{xy}^1\frac{\partial^4 w}{\partial x\,\partial y^3}+A_{xy}^0\frac{\partial^2\left(\frac{\partial w}{\partial x}\right)\left(\frac{\partial w}{\partial y}\right)}{\partial y^2}\end{array}\right)
\end{array}\right)\\
&+(ea)^2\\
&\left(\begin{array}{l}
A_{xy}^0\frac{\partial^3 u_0}{\partial x^2\partial y}+A_{xy}^0\frac{\partial^3 v_0}{\partial x^3}-2A_{xy}^1\frac{\partial^4 w}{\partial x^3\partial y}+A_{xy}^0\frac{\partial^2\left(\frac{\partial w}{\partial x}\right)\left(\frac{\partial w}{\partial y}\right)}{\partial x^2}\\
-\ell^2\left(\begin{array}{l}A_{xy}^0\frac{\partial^5 u_0}{\partial x^4\partial y}+A_{xy}^0\frac{\partial^5 v_0}{\partial x^5}-2A_{xy}^1\frac{\partial^6 w}{\partial x^5\partial y}+A_{xy}^0\frac{\partial^4\left(\frac{\partial w}{\partial x}\right)\left(\frac{\partial w}{\partial y}\right)}{\partial x^4}\\ +A_{xy}^0\frac{\partial^5 u_0}{\partial x^2\partial y^3}+A_{xy}^0\frac{\partial^5 v_0}{\partial x^3\partial y^2}-2A_{xy}^1\frac{\partial^6 w}{\partial x^3\partial y^3}+A_{xy}^0\frac{\partial^4\left(\frac{\partial w}{\partial x}\right)\left(\frac{\partial w}{\partial y}\right)}{\partial x^2\partial y^2}\end{array}\right)
\end{array}\right)
\end{aligned}
\tag{B-3}
$$

$$+(ea)^2$$

$$\left(\begin{array}{l} A_{xy}^0\dfrac{\partial^3 u_0}{\partial y^3}+A_{xy}^0\dfrac{\partial^3 v_0}{\partial x\,\partial y^2}-2A_{xy}^1\dfrac{\partial^4 w}{\partial x\,\partial y^3}+A_{xy}^0\dfrac{\partial^2\left(\dfrac{\partial w}{\partial x}\right)\left(\dfrac{\partial w}{\partial y}\right)}{\partial y^2} \\ -\ell^2\left(\begin{array}{l} A_{xy}^0\dfrac{\partial^5 u_0}{\partial x^2\partial y^3}+A_{xy}^0\dfrac{\partial^5 v_0}{\partial x^3\partial y^2}-2A_{xy}^1\dfrac{\partial^6 w}{\partial x^3\partial y^3}+A_{xy}^0\dfrac{\partial^4\left(\dfrac{\partial w}{\partial x}\right)\left(\dfrac{\partial w}{\partial y}\right)}{\partial x^2\partial y^2} \\ +A_{xy}^0\dfrac{\partial^5 u_0}{\partial y^5}+A_{xy}^0\dfrac{\partial^5 v_0}{\partial x\,\partial y^4}-2A_{xy}^1\dfrac{\partial^6 w}{\partial x\,\partial y^5}+A_{xy}^0\dfrac{\partial^4\left(\dfrac{\partial w}{\partial x}\right)\left(\dfrac{\partial w}{\partial y}\right)}{\partial y^4} \end{array}\right) \end{array}\right) \tag{B-3}$$

$$M_x=\frac{1}{1-\upsilon^2}\times$$

$$\left(\begin{array}{l} A_x^1\dfrac{\partial u_0}{\partial x}-A_x^2\dfrac{\partial^2 w}{\partial x^2}+A_x^1\dfrac{1}{2}(\dfrac{\partial w}{\partial x})^2+\upsilon\left(A_x^1\dfrac{\partial v_0}{\partial y}-A_x^2\dfrac{\partial^2 w}{\partial y^2}+A_x^1\dfrac{1}{2}(\dfrac{\partial w}{\partial y})^2\right) \\ -\ell^2\left(\begin{array}{l} A_x^1\dfrac{\partial^3 u_0}{\partial x^3}-A_x^2\dfrac{\partial^4 w}{\partial x^4}+A_x^1\dfrac{1}{2}\dfrac{\partial^2(\partial w/\partial x)^2}{\partial x^2}+\upsilon\left(\begin{array}{l} A_x^1\dfrac{\partial^3 v_0}{\partial x^2\partial y}-A_x^2\dfrac{\partial^4 w}{\partial x^2\partial y^2} \\ +A_x^1\dfrac{1}{2}\dfrac{\partial^2(\partial w/\partial y)^2}{\partial x^2}\end{array}\right) \\ +A_x^1\dfrac{\partial^3 u_0}{\partial x\,\partial y^2}-A_x^2\dfrac{\partial^4 w}{\partial x^2\partial y^2}+A_x^1\dfrac{1}{2}\dfrac{\partial^2(\partial w/\partial x)^2}{\partial y^2}+\upsilon\left(\begin{array}{l} A_x^1\dfrac{\partial^3 v_0}{\partial y^3}-A_x^2\dfrac{\partial^4 w}{\partial y^4} \\ +A_x^1\dfrac{1}{2}\dfrac{\partial^2(\partial w/\partial y)^2}{\partial y^2}\end{array}\right) \end{array}\right) \end{array}\right)$$

$$+\frac{(ea)^2}{1-\upsilon^2}\times \tag{B-4}$$

$$\left(\begin{array}{l} A_x^1\dfrac{\partial^3 u_0}{\partial x^3}-A_x^2\dfrac{\partial^4 w}{\partial x^4}+A_x^1\dfrac{1}{2}\dfrac{\partial^2(\partial w/\partial x)^2}{\partial x^2}+\upsilon\left(\begin{array}{l} A_x^1\dfrac{\partial^3 v_0}{\partial x^2\partial y}-A_x^2\dfrac{\partial^4 w}{\partial x^2\partial y^2} \\ +A_x^1\dfrac{1}{2}\dfrac{\partial^2(\partial w/\partial y)^2}{\partial x^2}\end{array}\right) \\ -\ell^2\left(\begin{array}{l} A_x^1\dfrac{\partial^5 u_0}{\partial x^5}-A_x^2\dfrac{\partial^6 w}{\partial x^6}+A_x^1\dfrac{1}{2}\dfrac{\partial^4(\partial w/\partial x)^2}{\partial x^4}+\upsilon\left(\begin{array}{l} A_x^1\dfrac{\partial^5 v_0}{\partial x^4\partial y}-A_x^2\dfrac{\partial^6 w}{\partial x^4\partial y^2} \\ +A_x^1\dfrac{1}{2}\dfrac{\partial^4(\partial w/\partial y)^2}{\partial x^4}\end{array}\right) \\ +A_x^1\dfrac{\partial^5 u_0}{\partial x^3\partial y^2}-A_x^2\dfrac{\partial^6 w}{\partial x^4\partial y^2}+A_x^1\dfrac{1}{2}\dfrac{\partial^4(\partial w/\partial x)^2}{\partial x^2\partial y^2} \\ +\upsilon\left(A_x^1\dfrac{\partial^5 v_0}{\partial x^2\partial y^3}-A_x^2\dfrac{\partial^6 w}{\partial x^2\partial y^4}+A_x^1\dfrac{1}{2}\dfrac{\partial^4(\partial w/\partial y)^2}{\partial x^2\partial y^2}\right) \end{array}\right) \end{array}\right)$$

$$
\begin{aligned}
&+\frac{(ea)^2}{1-\upsilon^2}\times\\
&\left(\begin{array}{l}
A_x^1\frac{\partial^3 v_0}{\partial y^3}-A_x^2\frac{\partial^4 w}{\partial y^4}+A_x^1\frac{1}{2}\frac{\partial^2(\partial w/\partial x)^2}{\partial y^2}+\upsilon\left(\begin{array}{l}A_x^1\frac{\partial^3 v_0}{\partial y^3}-A_x^2\frac{\partial^4 w}{\partial y^4}\\ +A_x^1\frac{1}{2}\frac{\partial^2(\partial w/\partial y)^2}{\partial y^2}\end{array}\right)\\
-t^2\left(\begin{array}{l}A_x^1\frac{\partial^5 u_0}{\partial x^3\partial y^2}-A_x^2\frac{\partial^6 w}{\partial x^4\partial y^2}+A_x^1\frac{1}{2}\frac{\partial^4(\partial w/\partial x)^2}{\partial x^2\partial y^2}+\upsilon\left(\begin{array}{l}A_x^1\frac{\partial^5 v_0}{\partial x^2\partial y^3}-A_x^2\frac{\partial^6 w}{\partial x^2\partial y^4}\\ +A_x^1\frac{1}{2}\frac{\partial^4(\partial w/\partial y)^2}{\partial x^2\partial y^2}\end{array}\right)\\ +A_x^1\frac{\partial^5 u_0}{\partial x\partial y^4}-A_x^2\frac{\partial^6 w}{\partial x^2\partial y^4}+A_x^1\frac{1}{2}\frac{\partial^4(\partial w/\partial x)^2}{\partial y^4}+\upsilon\left(\begin{array}{l}A_x^1\frac{\partial^5 v_0}{\partial y^5}-A_x^2\frac{\partial^6 w}{\partial y^6}\\ +A_x^1\frac{1}{2}\frac{\partial^4(\partial w/\partial y)^2}{\partial y^4}\end{array}\right)\end{array}\right)
\end{array}\right)\\
&-e_{31}\left(-C^1\beta'\phi_E-B^1\frac{2V_E}{h}\right)+\frac{(ea)^2}{1-\upsilon^2}\left(-e_{31}\left(-C^1\beta'\frac{\partial^2\phi_E}{\partial x^2}\right)-e_{31}\left(-C^1\beta'\frac{\partial^2\phi_E}{\partial y^2}\right)\right)
\end{aligned}
\tag{B-4}
$$

$$
\begin{aligned}
&M_y=\frac{1}{1-\upsilon^2}\times\\
&\left(\begin{array}{l}
A_y^1\frac{\partial v_0}{\partial y}-A_y^2\frac{\partial^2 w}{\partial y^2}+A_y^1\frac{1}{2}(\frac{\partial w}{\partial y})^2+\upsilon\left(A_x^1\frac{\partial u_0}{\partial x}-A_x^2\frac{\partial^2 w}{\partial x^2}+A_x^1\frac{1}{2}(\frac{\partial w}{\partial x})^2\right)\\
-t^2\left(\begin{array}{l}A_y^1\frac{\partial^3 v_0}{\partial x^2\partial y}-A_y^2\frac{\partial^4 w}{\partial x^2\partial y^2}+A_y^1\frac{1}{2}\frac{\partial^2(\partial w/\partial y)^2}{\partial x^2}+\upsilon\left(\begin{array}{l}A_x^1\frac{\partial^3 u_0}{\partial x^3}-A_x^2\frac{\partial^4 w}{\partial x^4}\\ +A_x^1\frac{1}{2}\frac{\partial^2(\partial w/\partial x)^2}{\partial x^2}\end{array}\right)\\ +A_y^1\frac{\partial^3 v_0}{\partial y^3}-A_y^2\frac{\partial^4 w}{\partial y^4}+A_y^1\frac{1}{2}\frac{\partial^2(\partial w/\partial y)^2}{\partial y^2}+\upsilon\left(\begin{array}{l}A_x^1\frac{\partial^3 u_0}{\partial x\partial y^2}-A_x^2\frac{\partial^4 w}{\partial x^2\partial y^2}\\ +A_x^1\frac{1}{2}\frac{\partial^2(\partial w/\partial x)^2}{\partial y^2}\end{array}\right)\end{array}\right)
\end{array}\right)\\
&+\frac{(ea)^2}{1-\upsilon^2}\times\\
&\left(\begin{array}{l}
A_y^1\frac{\partial^3 v_0}{\partial x^2\partial y}-A_y^2\frac{\partial^4 w}{\partial x^2\partial y^2}+A_y^1\frac{1}{2}\frac{\partial^2(\partial w/\partial y)^2}{\partial x^2}+\upsilon\left(\begin{array}{l}A_x^1\frac{\partial^3 u_0}{\partial x^3}-A_x^2\frac{\partial^4 w}{\partial x^4}\\ +A_x^1\frac{1}{2}\frac{\partial^2(\partial w/\partial x)^2}{\partial x^2}\end{array}\right)\\
-t^2\left(\begin{array}{l}A_y^1\frac{\partial^5 v_0}{\partial x^4\partial y}-A_y^2\frac{\partial^6 w}{\partial x^4\partial y^2}+A_y^1\frac{1}{2}\frac{\partial^4(\partial w/\partial y)^2}{\partial x^4}+\upsilon\left(\begin{array}{l}A_x^1\frac{\partial^5 u_0}{\partial x^5}-A_x^2\frac{\partial^6 w}{\partial x^6}\\ +A_x^1\frac{1}{2}\frac{\partial^4(\partial w/\partial x)^2}{\partial x^4}\end{array}\right)\\ +A_y^1\frac{\partial^5 v_0}{\partial x^2\partial y^3}-A_y^2\frac{\partial^6 w}{\partial x^2\partial y^4}+A_y^1\frac{1}{2}\frac{\partial^4(\partial w/\partial y)^2}{\partial x^2\partial y^2}+\upsilon\left(\begin{array}{l}A_x^1\frac{\partial^5 u_0}{\partial x^3\partial y^2}-A_x^2\frac{\partial^6 w}{\partial x^4\partial y^2}\\ +A_x^1\frac{1}{2}\frac{\partial^4(\partial w/\partial x)^2}{\partial x^2\partial y^2}\end{array}\right)\end{array}\right)
\end{array}\right)
\end{aligned}
\tag{B-5}
$$

$$
\begin{aligned}
&+\frac{(ea)^2}{1-\upsilon^2}\times\left(\begin{array}{l}
A_y^1\frac{\partial^3 v_0}{\partial y^3}-A_y^2\frac{\partial^4 w}{\partial y^4}+A_y^1\frac{1}{2}\frac{\partial^2(\partial w/\partial y)^2}{\partial y^2}+\upsilon\left(\begin{array}{l}A_x^1\frac{\partial^3 u_0}{\partial x\partial y^2}-A_x^2\frac{\partial^4 w}{\partial x^2\partial y^2}\\ +A_x^1\frac{1}{2}\frac{\partial^2(\partial w/\partial x)^2}{\partial y^2}\end{array}\right)\\
-\ell^2\left(\begin{array}{l}A_y^1\frac{\partial^5 v_0}{\partial x^2\partial y^3}-A_y^2\frac{\partial^6 w}{\partial x^2\partial y^4}+A_y^1\frac{1}{2}\frac{\partial^4(\partial w/\partial y)^2}{\partial x^2\partial y^2}+\upsilon\left(\begin{array}{l}A_x^1\frac{\partial^5 u_0}{\partial x^3\partial y^2}-A_x^2\frac{\partial^6 w}{\partial x^4\partial y^2}\\ +A_x^1\frac{1}{2}\frac{\partial^4(\partial w/\partial x)^2}{\partial x^2\partial y^2}\end{array}\right)\\
+A_y^1\frac{\partial^5 v_0}{\partial y^5}-A_y^2\frac{\partial^6 w}{\partial y^6}+A_y^1\frac{1}{2}\frac{\partial^4(\partial w/\partial y)^2}{\partial y^4}+\upsilon\left(\begin{array}{l}A_x^1\frac{\partial^5 u_0}{\partial x\partial y^4}-A_x^2\frac{\partial^6 w}{\partial x^2\partial y^4}\\ +A_x^1\frac{1}{2}\frac{\partial^4(\partial w/\partial x)^2}{\partial y^4}\end{array}\right)\end{array}\right)
\end{array}\right)\\
&-e_{32}\left(-C^1\beta'\phi_E-B^1\frac{2V_E}{h}\right)+\frac{(ea)^2}{1-\upsilon^2}\left(-e_{32}\left(-C^1\beta'\frac{\partial^2\phi_E}{\partial x^2}\right)-e_{32}\left(-C^1\beta'\frac{\partial^2\phi_E}{\partial y^2}\right)\right)
\end{aligned}
\tag{B-5}
$$

$$
M_{xy}=
\left(\begin{array}{l}
A_{xy}^1\frac{\partial u_0}{\partial y}+A_{xy}^1\frac{\partial v_0}{\partial x}-2A_{xy}^2\frac{\partial^2 w}{\partial x\partial y}+A_{xy}^1\left(\frac{\partial w}{\partial x}\right)\left(\frac{\partial w}{\partial y}\right)\\
-\ell^2\left(A_{xy}^1\frac{\partial^3 u_0}{\partial x^2\partial y}+A_{xy}^1\frac{\partial^3 v_0}{\partial x^3}-2A_{xy}^2\frac{\partial^4 w}{\partial x^3\partial y}+A_{xy}^1\frac{\partial^2\left(\frac{\partial w}{\partial x}\right)\left(\frac{\partial w}{\partial y}\right)}{\partial x^2}+A_{xy}^1\frac{\partial^3 u_0}{\partial y^3}+A_{xy}^1\frac{\partial^3 v_0}{\partial x\partial y^2}-2A_{xy}^2\frac{\partial^4 w}{\partial x\partial y^3}+A_{xy}^1\frac{\partial^2\left(\frac{\partial w}{\partial x}\right)\left(\frac{\partial w}{\partial y}\right)}{\partial y^2}\right)
\end{array}\right)
$$

$$
\begin{aligned}
&+(ea)^2\\
&\left(\begin{array}{l}
A_{xy}^1\frac{\partial^3 u_0}{\partial x^2\partial y}+A_{xy}^1\frac{\partial^3 v_0}{\partial x^3}-2A_{xy}^2\frac{\partial^4 w}{\partial x^3\partial y}+A_{xy}^1\frac{\partial^2\left(\frac{\partial w}{\partial x}\right)\left(\frac{\partial w}{\partial y}\right)}{\partial x^2}\\
-\ell^2\left(A_{xy}^1\frac{\partial^5 u_0}{\partial x^4\partial y}+A_{xy}^1\frac{\partial^5 v_0}{\partial x^5}-2A_{xy}^2\frac{\partial^6 w}{\partial x^5\partial y}+A_{xy}^1\frac{\partial^4\left(\frac{\partial w}{\partial x}\right)\left(\frac{\partial w}{\partial y}\right)}{\partial x^4}+A_{xy}^1\frac{\partial^5 u_0}{\partial x^2\partial y^3}+A_{xy}^1\frac{\partial^5 v_0}{\partial x^3\partial y^2}-2A_{xy}^2\frac{\partial^6 w}{\partial x^3\partial y^3}+A_{xy}^1\frac{\partial^4\left(\frac{\partial w}{\partial x}\right)\left(\frac{\partial w}{\partial y}\right)}{\partial x^2\partial y^2}\right)
\end{array}\right)
\end{aligned}
\tag{B-6}
$$

$$
\begin{aligned}
&+(ea)^2\\
&\left(\begin{array}{l}
A_{xy}^1\frac{\partial^3 u_0}{\partial y^3}+A_{xy}^1\frac{\partial^3 v_0}{\partial x\partial y^2}-2A_{xy}^2\frac{\partial^4 w}{\partial x\partial y^3}+A_{xy}^1\frac{\partial^2\left(\frac{\partial w}{\partial x}\right)\left(\frac{\partial w}{\partial y}\right)}{\partial y^2}\\
-\ell^2\left(A_{xy}^1\frac{\partial^5 u_0}{\partial x^2\partial y^3}+A_{xy}^1\frac{\partial^5 v_0}{\partial x^3\partial y^2}-2A_{xy}^2\frac{\partial^6 w}{\partial x^3\partial y^3}+A_{xy}^1\frac{\partial^4\left(\frac{\partial w}{\partial x}\right)\left(\frac{\partial w}{\partial y}\right)}{\partial x^2\partial y^2}+A_{xy}^1\frac{\partial^5 u_0}{\partial y^5}+A_{xy}^1\frac{\partial^5 v_0}{\partial x\partial y^4}-2A_{xy}^2\frac{\partial^6 w}{\partial x\partial y^5}+A_{xy}^1\frac{\partial^4\left(\frac{\partial w}{\partial x}\right)\left(\frac{\partial w}{\partial y}\right)}{\partial y^4}\right)
\end{array}\right)
\end{aligned}
$$

$$
\begin{aligned}
\overline{D}_x &= \xi_{11} D^0 \frac{\partial \phi_E}{\partial x} + (ea)^2 \left(\xi_{11} D^0 \frac{\partial^3 \phi_E}{\partial x^3} + \xi_{11} D^0 \frac{\partial^3 \phi_E}{\partial x \partial y^2} \right) \\
\overline{D}_y &= \xi_{22} D^0 \frac{\partial \phi_E}{\partial y} + (ea)^2 \left(\xi_{22} D^0 \frac{\partial^3 \phi_E}{\partial x^2 \partial y} + \xi_{22} D^0 \frac{\partial^3 \phi_E}{\partial y^3} \right) \\
\overline{D}_z &= e_{31} \left(B^0 \frac{\partial u_0}{\partial x} - B^1 \frac{\partial^2 w}{\partial x^2} + B^0 \frac{1}{2} (\frac{\partial w}{\partial x})^2 \right) \\
&+ e_{32} \left(B^0 \frac{\partial v_0}{\partial y} - B^1 \frac{\partial^2 w}{\partial y^2} + B^0 \frac{1}{2} (\frac{\partial w}{\partial y})^2 \right) + \xi_{33} \left(-\beta' C^0 \phi_E - B^0 \frac{2V_E}{h} \right) \\
&+ (ea)^2 \left(\begin{array}{l} e_{31} \left(B^0 \frac{\partial^3 u_0}{\partial x^3} - B^1 \frac{\partial^4 w}{\partial x^4} + B^0 \frac{1}{2} \frac{\partial^2 (\frac{\partial w}{\partial x})^2}{\partial x^2} \right) \\ + e_{32} \left(B^0 \frac{\partial^3 v_0}{\partial x^2 \partial y} - B^1 \frac{\partial^4 w}{\partial x^2 \partial y^2} + B^0 \frac{1}{2} \frac{\partial^2 (\frac{\partial w}{\partial y})^2}{\partial x^2} \right) + \xi_{33} \left(-\beta' C^0 \frac{\partial^2 \phi_E}{\partial x^2} \right) \end{array} \right) \\
&+ (ea)^2 \left(\begin{array}{l} e_{31} \left(B^0 \frac{\partial^3 u_0}{\partial x \partial y^2} - B^1 \frac{\partial^4 w}{\partial x^2 \partial y^2} + B^0 \frac{1}{2} \frac{\partial^2 (\frac{\partial w}{\partial x})^2}{\partial y^2} \right) \\ + e_{32} \left(B^0 \frac{\partial^3 v_0}{\partial y^3} - B^1 \frac{\partial^4 w}{\partial y^4} + B^0 \frac{1}{2} \frac{\partial^2 (\frac{\partial w}{\partial y})^2}{\partial y^2} \right) + \xi_{33} \left(-\beta' C^0 \frac{\partial^2 \phi_E}{\partial y^2} \right) \end{array} \right)
\end{aligned}
\tag{B-7}
$$

Appendix C

Using Eq. (21), we consider the variation of strain energy into two parts including mechanical and electrical fields as follows:

$$\delta U = \delta U_M + \delta U_E \tag{C-1}$$

where

$$\delta U_M = \int_A \int_{-\frac{h}{2}}^{\frac{h}{2}} (\sigma_{xx} \delta \varepsilon_{xx} + \sigma_{yy} \delta \varepsilon_{yy} + \tau_{xy} \delta \gamma_{xy}) dz dA \tag{C-2}$$

$$\delta U_E = \int_A \int_{-\frac{h}{2}}^{\frac{h}{2}} (-D_x \delta E_x - D_y \delta E_y - D_z \delta E_z) dz dA \tag{C-3}$$

Substituting Eq. (9) into Eq. (C-2), we have:

$$
\begin{aligned}
\delta U_M = \int_A \int_{-\frac{h}{2}}^{\frac{h}{2}} (&\sigma_{xx} \delta (u_{0,x} - z w_{,xx}) + \sigma_{yy} \delta (v_{0,y} - z w_{,yy}) \\
&+ \tau_{xy} \delta (u_{0,y} + v_{0,x} - 2 z w_{,xy})) dz dA
\end{aligned}
\tag{C-4}
$$

Substituting Eq. (22) into Eq. (C-4), the following equation is obtained:

$$
\begin{aligned}
\delta U_M = \int_A (&N_x \delta u_{0,x} - M_x \delta w_{,xx} + N_y \delta v_{0,y} - M_y \delta w_{,yy} \\
&+ N_{xy} \delta (u_{0,y} + v_{0,x}) - 2 M_{xy} \delta w_{,xy}) dA
\end{aligned}
\tag{C-5}
$$

After simplifying and using variational method, the variation of strain energy for mechanical part is written as :

$$
\begin{aligned}
\delta U_M = &\int_0^b ((N_x \delta u_0)_0^a + (N_{xy} \delta v_0)_0^a) dy \\
&\int_0^a ((N_y \delta v_0)_0^b + (N_{xy} \delta u_0)_0^b) dx \\
&\int_0^b (-(M_x \delta w_{,x})_0^a + (M_{x,x} \delta w)_0^a - 2(M_{xy} \delta w_{,y})_0^a) dy \\
&\int_0^a (-(M_y \delta w_{,y})_0^b + (M_{y,y} \delta w)_0^b + 2(M_{xy,x} \delta w)_0^b) dy \\
&\int_A (-N_{x,x} \delta u_0 - M_{x,xx} \delta w - N_{y,y} \delta v_0 \\
&- M_{y,yy} \delta w - N_{xy,y} \delta u_0 - N_{xy,x} \delta v_0 - 2 M_{xy,xy} \delta w) dA
\end{aligned}
\tag{C-6}
$$